Preliminary Aerodynamic Investigation of Box-Wing Configurations using Low Fidelity Codes

FAHAD AMAN KHAN

Master's Thesis
Luleå University of Technology
Dept. of Space Science, Kiruna

This thesis was conducted at the ***Aircraft Design and System Group* – Aero**, Department of Automotive and Aeronautical Engineering at Hamburg University of Applied Sciences in corporation with Luleå Tekniska Universitet and Université Paul Sabatier Toulouse III

Statutory Declaration

"I declare in lieu of an oath that I have written this diploma thesis myself and that I have not used any sources or resources other than stated for its preparation. I further declare that I have clearly indicated all direct and indirect quotations. This master thesis has not been submitted elsewhere for examination purposes."

May 08, 2010   Fahad Aman Khan
Hamburg, Germany

Abstract

This work outlines the different aerodynamic aspects of box-wing design i.e. an unconventional aircraft design configuration exhibiting the capability of reducing induced drag. Being a nonplanar concept, the basic aerodynamic features differ from conventional designs.

To understand these features and their influence on box-wing aerodynamics, parameter variations have been conducted while Munk's theorem is validated for stagger and sweep. In this process, several important aspects of box-wing are highlighted. An optimization algorithm has been implemented by considering all the design variables collectively to find the global maximum for the box-wing design. All these investigations laid down the important aerodynamic features of box-wing and also proved a method for estimating the reduction in induced drag.

To conduct these investigations, vortex lattice methods (VLM) are used. Nonplanar systems have certain limitations for best operations which provide maximum induced drag reduction. These limitations are examined and applied in the form of constant and specified lift distributions in the analysis. Furthermore, it is concluded that vortex lattice methods do capture the reduction in induced drag correctly if the limitations of span loading are maintained during the analysis.

Based on previous results obtained, Euler inviscid analysis for a selected box-wing and a reference wing are carried out. The results of Euler inviscid analysis show good agreement with the results achieved by vortex lattice method in drag reduction. Therefore, VLM methods are capable of analyzing box-wing (and multi planar systems) to a good accuracy. At the same time, transonic airfoil selection is identified as one of the key factors in designing a commercial box-wing aircraft.

This study is closed up by discussing different potential advantages for the aviation industry and discusses if a box-wing commercial aircraft should be made reality.

On the whole, this work looks into a possible way of investigating futuristic multi planar aircraft configurations by using low fidelity aerodynamic codes.

Acknowledgements

Table of Contents

Notations and Abbreviations

AR	Aspect Ratio
b	Span
C_D	Coefficient of Drag
C_L	Coefficient of Lift
C_{Dc}	Coefficient of Compressibility Drag
C_{Di}	Coefficient of Induced Drag
D	Drag
e	Oswald's / Span Efficiency Factor
FAA	Federal Aviation Administration
h	Height (Vertical distance between main wings of box-wing)
$ICAO$	International Civil Aviation Organization
MAC	Mean Aerodynamic Chord
S_{ref}	Reference Wing Area
V_{CR}	Cruise Velocity
VLA	Very Large Aircraft
VLM	Vortex Lattice Method

List of Figures

x

List of Tables

1 Introduction

Air traffic is predicted to grow at a rate of 5% annually, resulting in a rapid increase of carbon emissions for aviation industry. Combined with uncertainties of aviation contributions to climate change, there has never been such a tremendous need for improved and efficient civil transport aircrafts. The "Vision for 2020" by ACARE (European Aeronatics: A Vision For 2020, January 2001) is a research agenda which outlines: cost reduction, environment, safety and security as the most important factors for the aviation industry by year 2020.

A study having similar aims is being carried out in the *Airport 2030* project. This project is lead by **German Aerospace Centre (DLR)** in Hamburg. *Airport 2030* looks into the future airport designs in accordance with the upcoming aircraft design trends. Under its framework, the **Aircraft Design and System Group (Aero)** investigates different aircraft design modifications that exhibit advantages in operations, both on and off ground. The box-wing design is one of the nonplanar concepts having its origins from early days of aviation and is also being studied as part of the *Airport 2030* project.

Current conventional aircrafts are designed and optimized to achieve highest levels of performance and it would be extremely difficult to come up with the new design solutions for the future out of the existing trends. Likewise, summarizing their work in the International Congress of the Aeronautical Sciences, Mistry, Smith and Fielding (Smith, 2008) emphasized that significant reduction in noise, fuel and cost in future can only be made by adopting novel concepts.

One of the major advantages obtained from novel concepts like the nonplanar box-wing design, is a reduction in drag compared with planar wings of same span and lift (Kroo I. , 2005). Drag reduction results in a direct decrease in operating costs and in an in-direct decrease in noise and emissions levels. Drag during the cruise phase of large transport aircraft consist of friction and induced drag, where the induced drag is relatively lower than the friction drag. But still it consists of 43% of the total drag budget (Frediani, 2006). Thus, any reduction in the induced drag will directly improve the efficiency of the overall design. Moreover induced drag is also coupled with viscous or friction drag (Kroo I. , 2005), thus its reduction can be beneficial in a greater extent than actually comprehended.

Thus, this study is primarily based on finding an insight into the unique aerodynamic characteristics of box-wing configurations, with aims to outline and capture the important factors of the design for drag reduction which can consequently lead to performance improvements.

2 Literature Review

This study begins with a brief introduction of aircraft drag and its types. Afterwards fundamentals of vortex or induced drag are explained and possible mitigation techniques are highlighted.

The chapter further extends to develop an understanding for different nonplanar concepts and their applications with respect to an induced drag reduction. Furthermore, previous studies of box-wing designs are presented and discussed. Recent developments in this field are highlighted along with the several possible benefits as well as problems to deal with in the future.

2.1 Concept of Drag

Drag is the aerodynamic force that opposes an aircraft's motion through the air. From the early days of aviation, aerodynamicists have been trying to minimize the drag by direct and in-direct methods. Some of these techniques will be highlighted in the following chapters.

Mathematically drag is defined as:

$$D = \frac{\rho V^2 S_{ref} C_D}{2}$$

(2.1)

Where; ρ= Density, V= Velocity, S_{ref}= Reference Surface Area and C_D= Coefficient of Drag

Drag is the heart of aerodynamic design of an aircraft. As it equals the power required from the propulsion system of the aircraft during its cruise stage (for civil transport aircraft the cruise segment comprises almost 90% of flight time). Thus it directly corresponds to the amount of power required, fuel consumed and resultantly the overall weight of the aircraft. Higher drag means lower performance, as can be seen by an example: on the Concorde, one drag count increase ($\Delta C_D = 0.0001$) requires two passengers to be taken off, out of the 90 ~ 100 passenger capacity, during the North Atlantic run (Strang, 1979).

The coefficient of drag (C_D) is a dimensionless quantity, which quantifies the drag or resistance a particular aircraft has. Lower values indicate a "cleaner" design.

2.2 Types of Drag

When defining the types of drag, several viewpoints are present, depending upon the type of reader or the nature of analysis that is to be carried out. Here, types of drag are defined in context of *fluid mechanics*, as follows:

- Parasite Drag
- Induced Drag
- Compressibility Drag

Mathematically in coefficient form, these types can be written as (Kroo I. , 2001):

$$C_D = D \Big/ \frac{1}{2}\rho V^2 S_{ref} = C_{D_p} + {C_L}^2 \Big/ \pi e AR + \Delta C_{D_c}$$

(2.2)

Where; AR = Aspect Ratio, e = Oswald's or span efficiency factor, C_L = Design lift coefficient

Parasite drag (C_{D_p}) consists primarily of skin friction and pressure drag associated with viscosity. It is a direct function of aircraft wetted area and its aerodynamic contouring. Whereas, induced drag accounts the losses associated with generation in lift. This form of drag will be explained in more detail in the next section. The last term contributes to the increase in drag due to compressibility effects (ΔC_{D_c}) when an aircraft enters the transonic flow regimes.

2.3 Induced Drag

Lift is generated by the pressure differential created by the airfoil section along the span of the wing. As shown in figure 2.1 below, for finite wings (3D flow) this pressure differential causes the flow at wing tips to curl around and thus forming circular flow near the wing tips, which results in generation of wingtip vortices.
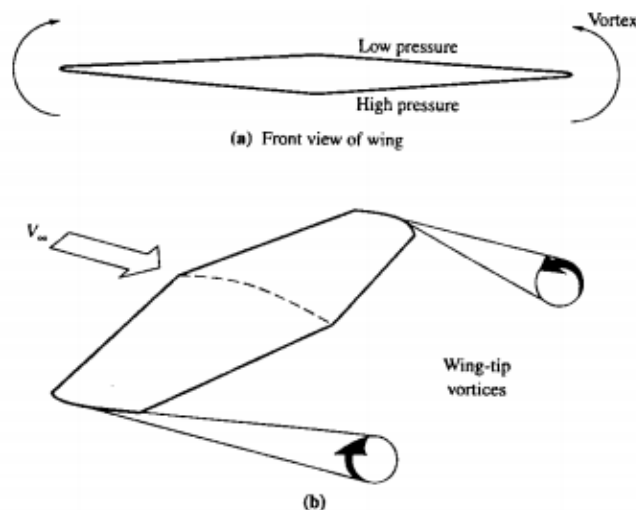
Figure 2.1 - Wing tip vortices (Anderson J. D., 1999)

3

This vortex system in-return causes a downward component of velocity along the span called *downwash*. The downwash combined with free stream relative to wind velocity, reduces the effective angle of attack along the span as shown in figure 2.2 below:
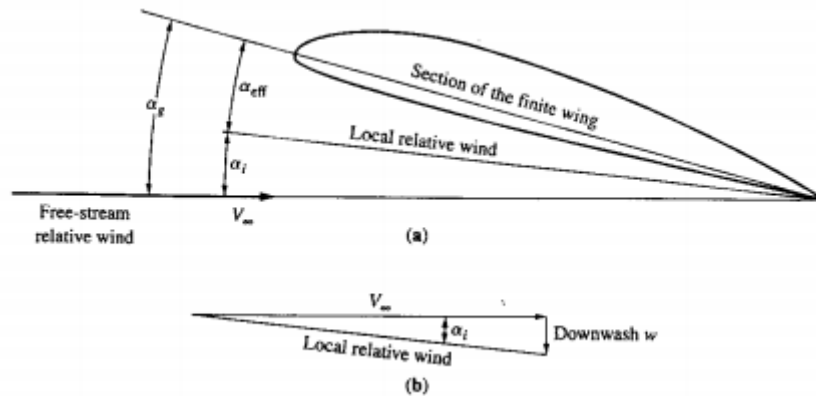
Figure 2.2 - Illustration of induced and effective angle of attack caused by downwash (Anderson J. D., 1999)

This reduction in angle of attack results in a local inclination of the lift vector relative to the incoming velocity vector and produces an *induced drag* (Mason, 1995).

For a closer look into induced drag, equation 2.2 for induced drag component can be separately written as:

$$C_{D_i} = {C_L}^2 / {\pi e AR}$$

(2.3)

Here, *e* is called Oswald's efficiency factor or span efficiency factor and accounts for the nonoptimal lift distribution along the span. According to (Munk, 1921), minimum induced drag for a planar wing of fixed total lift and span can be achieved with a distribution of wake-induced downwash that is constant in the far wake (Kroo I. , 2001). To attain this condition the lift distribution over the span should follow an elliptical shape. In this case the span efficiency factor becomes unity. Following the discussion above and the equation 2.3, two possible ways of induced drag reduction are obvious. These will be discussed in the next section separately.

From equation 2.2, it can be seen that the coefficient of drag depends mainly upon parasite and induced drag while compressibility drag is only present in the transonic flight regime and thus has a considerably lesser contribution to the complete drag budget. Neglecting the compressibility drag, the drag equation can be written as:

$$D = qS_{ref}C_{D_p} + \left.qS_{ref}C_L{}^2\middle/\pi e AR\right.$$

Where; q = dynamic pressure $\left({}^1\!/_2\,\rho V^2\right)$

Above equation shows that drag will be minimized at the speed where induced drag would be equal to the parasite drag. In other words, induced drag roughly accounts for half of the total drag when the aircraft is flying at its best lift to drag ratio. For civil transport aircrafts, this speed is lesser than their normal cruising speed. Nevertheless, induced drag still contributes to 43% of the total drag during cruise (Frediani, 2006).

For other flight segments, like takeoff, climb and landing for a typical civil transport, the aircraft lift coefficient is increased by several times. As induced drag is mainly dependent on operating lift coefficient and thus at these flight segments the contribution of the induced drag rises even more than the parasite drag. This can be seen in the equation above, the parasite drag decreases with decrease in flight speed. Alternatively induced drag increases with higher lift coefficients are needed at lower flight speeds to keep the aircraft in air.

Thus it can be seen that by a reduction in induced drag the aircraft can benefit in all segments of its flight and not only in the cruise stage. As aircrafts are designed in keeping all the segments of operation in similar perspective, an induced drag reduction also occurs e.g. during take-off and it will change conditions associated with engine-out climb. Changes in aircraft performance at these conditions influence the overall design and thus have an indirect, but powerful effect on the aircraft cruise performance (Kroo I. , 2001).

2.3.1 Induced Drag Reduction Techniques

From the previous discussion, it can be seen that an induced drag reduction can be carried out by increasing the aspect ratio and the span efficiency factor.

Increasing the aspect ratio means increasing the span of the wing while keeping the reference area constant. With the increase in span, the vortex strength along the tips is decreased and consequently the reduction in effective angle of attack is less compared to small aspect ratio wings. Robert T. Jones showed in his report on minimization of induced drag that a 15% induced drag reduction is possible with a 15% increase in span (Jones, 1950).

Although increasing span has aerodynamic benefits, structurally it is not the best option, as its increase results in aero elastic problems of the wing. The centre of lift moves away from the root of the wing, resulting in the need of a stronger internal structure to compensate the additional forces. In return, to make the structure stronger, additional mass is added to the

aircraft, which in itself reduces the overall performance of the design. Another problem which has surfaced due to increase in span is airport terminal restrictions. Currently the maximum space allotted for aircraft parking at terminals is an 80x80 m box. The Airbus A380 has a span of 79.8m just shy of the 80m box limit. If the wing loading for the Airbus A380 would be similar to that of an Airbus A340 it would have resulted in a span of 102m, which as a result would improve the performance along with a decrease in specific fuel consumption and wing area (Collins, 2001). Thus it can be observed that the increase in span has its benefits but the hurdles associated with it make it a challenging task.

Another way to reduce the induced drag is by increasing the span efficiency factor. As mentioned before for a planar wing having a given span and lift, the maximum span efficiency factor is limited to unity. For nonplanar systems span efficiency factor can be increased beyond unity. For the same span and total lift, nonplanar surfaces can significantly reduce induced drag as compared to a planar wing. The section below gives the general ideas behind the nonplanar concepts.

2.4 Nonplanar Concepts for Induced Drag Reduction

Nonplanar concepts have been present from the start of aviation. The first aircraft to fly by the Wright brothers was a nonplanar design: a *biplane*. Although at that time, the structural benefit obtained out of the biplane design was of more importance than the aerodynamic aspects of the design.

Several nonplanar concepts are shown in figure 2.3. It shows the front views of different wing layouts. It can be seen that the box-wing configuration shown in bottom right has the maximum span efficiency out of all configurations shown.
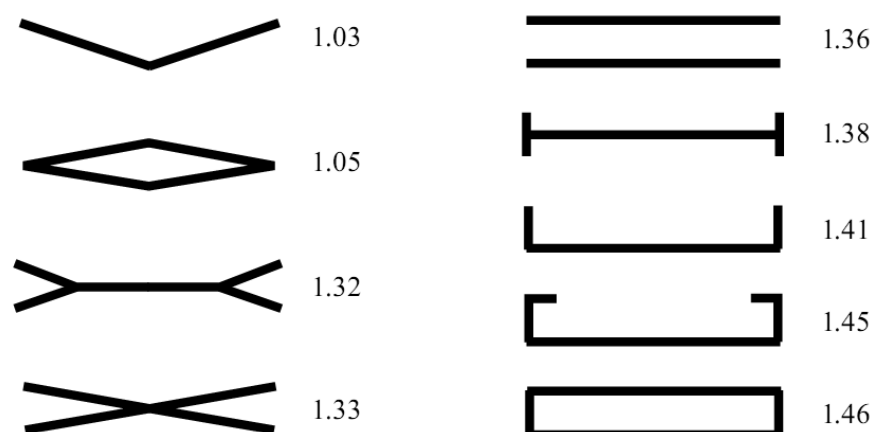
Figure 2.3 - Span efficiencies for various optimally loaded nonplanar system (*h/b=0.2*) (Kroo I. , 2001)

Some of the layouts take advantage of reduction in induced drag by end plates (or winglets) at wing tips. Others have an increased aspect ratio for individual wings by distributing one wing into multiple wings having same span and same total area. For box-wing configuration, it takes advantage from both aspects. These aspects will be discussed in the next section in more detail.

These results were obtained with a height to span ratio of 0.2. If this ratio is increased, the span efficiencies can even go higher as shown in figure 2.4 because the mutual interference drag reduces as the gap between the lifting surfaces is increased (Kroo I. , 2005).
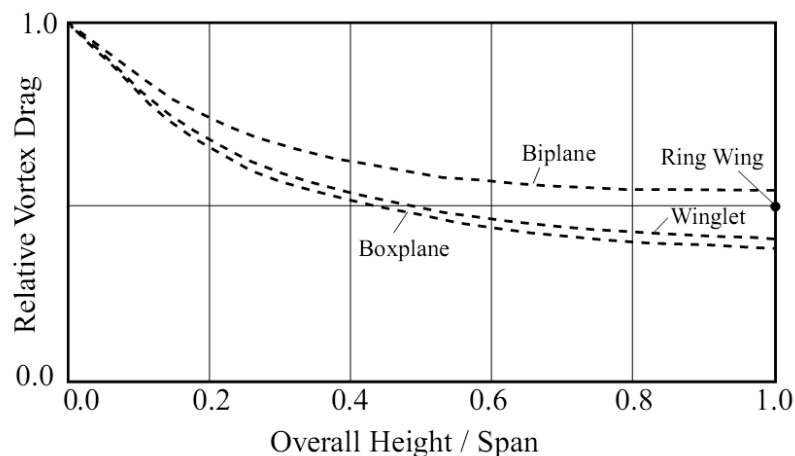
Figure 2.4 - Induced drag variation with allowable height for nonplanar systems (Kroo I. , 2005)

Several of the concepts shown in figure 2.3 above, have been transformed into successful aircrafts over the years. For example Rutan *Quickie* is based on a multiple wing design concept. Recently, the addition of winglets has been very popular which lies also in domain of nonplanar designs. Several commercial aircrafts from business jets to airliners have installed winglets to reduce induced drag by decreasing strength of the wing tip vortex.

2.5 Prandtl Best Wing System

In his paper in 1924, L. Prandtl presented the idea of best wing system based on the biplane concept.

According to his findings, the biplane has lesser drag than an equivalent monoplane and its minimum drag is obtained when two wings of biplane are of same span (Prandtl, 1924). Further on, more reduction in induced drag is possible if wing end plates are attached to the wing tips thus making it a closed system, as shown in figure 2.5.
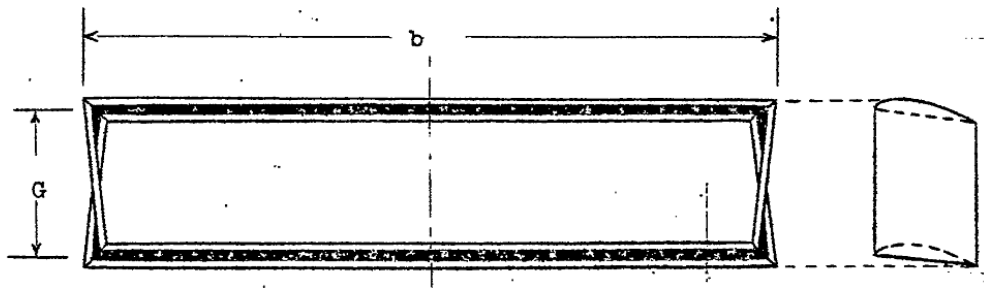
Figure 2.5 - Prandtl's best wing system, front and side views (Prandtl, 1924)

To utilize the usefulness of best wing system it must have same lift distribution and same total lift on each of the horizontal wings and butterfly shaped lift distribution on the vertical tip wings. When these conditions of minimum occur, the velocity induced by the free vortices is constant along the two horizontal wings and identically zero on the vertical side wings. The induced drag decreases for increasing non-dimensional gap (A. Frediani, 2005).

In addition to reductions in induced drag, the box-wing configuration has desirable effects on structures, stability and control characteristics, vortex wake hazards, and other practical aspects of the design (Kroo I. , 2005).

2.6 Munk's Stagger Theorem

Munk (Munk, 1921) addressed many aspects of nonplanar systems in his NACA document TN 921. In his report, he solved the local induced velocity on each surface to evaluate the induced drag of wing systems. Furthermore, he showed how the interference drag on each surface varied as the longitudinal separation between elements was changed. One of his interesting results is that if the circulation of each element in wing systems is kept constant, than the total induced drag of the system will remain the same. In other words the induced drag is independent of the longitudinal position of the lifting surface as long as the total circulation for each surface is held constant. This has become known as Munk's stagger theorem and is of great importance in evaluating concepts for induced drag reduction (Kroo I. , 2001).

Figure 2.6, shows the illustration of Munk's theorem. Given that the lift distribution denoted by L_1, L_2 and L_3 along span remains the same, the stagger or sweep has no effect on the induced drag of the complete system.

8
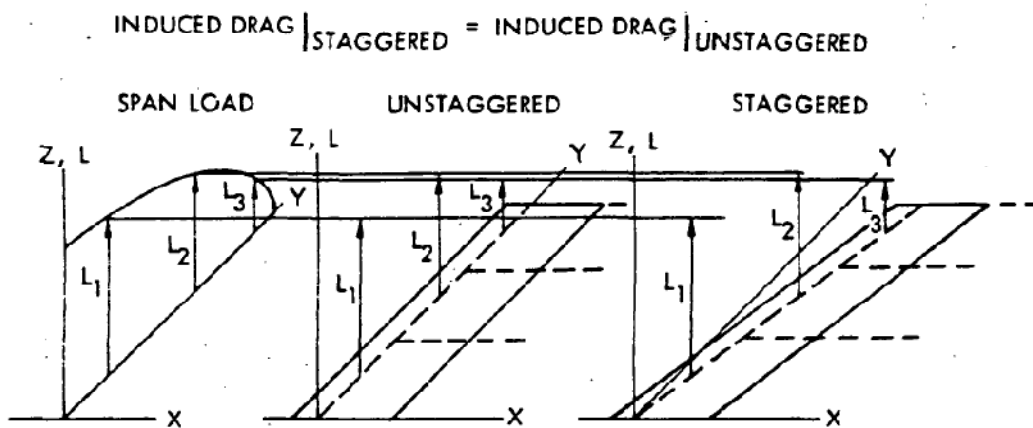
Figure 2.6 - Illustration of Munk's stagger theorem (Gall, 1984)

By applying Munk's stagger theorem on box-wing configuration, can be concluded that the induced drag of the system is independent of the stagger between the two horizontal wings. In other words, the two wings can be moved and placed horizontally at any position as long as the lift circulation of the two wings is kept the same by changing the incidence of individual wings. Another important aspect which should be mentioned here is that, the sweep has similarly no effect on induced drag in box-wing configuration as long as the front view of the configuration is kept the same. This second effect enables the aerodynamicist to design a transonic configuration of a box-wing for which wing sweep has important implications (A. Frediani, 2005).

2.7 Physical Interpretation of a Nonplanar System

If the box-wing configuration is studied more carefully it can be seen that it is a combination of two wings having winglets attached at their tips. The lower wing has a winglet which has a 0° cant angle (right angled, upward) while the upper wing has a winglet with 180° cant angle (right angled, downward) such that both winglets are connected at their tips. Furthermore, the lift distribution for winglets described in the section *Prandtl's Best Wing System,* states that lift goes to zero at the point where the two winglets meet. Thus, we can try to understand the box-wing system by analyzing a single wing with a pair of winglet attached at its tips. For this purpose the following explanation is taken from (Gall, 1984).

Figure 2.7 shows the sources of induced drag for a wing-winglet combination. These can be summarized as:

- Induced drag due to the induced flow by the wings on the wing (Figure 2.7a)
- Induced drag due to the induced flow by the wings on the winglet (Figure 2.7b)

9

- Induced drag due to the induced flow by the winglets on the wing (Figure 2.7c)
- Induced drag due to the induced flow by the winglets on the winglet (Figure 2.7d)

In figure 2.7a, the effect of induced flow on a wing by itself is shown. It is similar to figure 2.2 and its discussion. The main wing is producing a downwash w_w on itself because of the inclination of the lift vector F. In addition to this, the winglet is producing a sidewash (downwash of winglet in sideways) on the main wing.

Figure 2.7b, drag due to wing on winglet is shown. The sidewash of the winglet combines with freestream velocity and produces a forward force component. This can be called as *induced force (Di)*. The direction of freestream velocity at the winglet is tilted forward because of the 3-dimensional circular flow near the tips which forces the incoming velocity vector to change its direction.

Similarly in 2.7c, the induced drag resulting from the sidewash induced by the winglet on itself is presented. It is similar to Figure 2.7a, the effective angle of attack gets reduced which is creating an induced drag on the winglet itself. Here it should be noted that the winglet is loaded inwards. The winglet also induces an upwash on the wing (*wl*).

(a) Drag due to wing on wing $D_{i_{w.w}}$.   (b) Drag due to wing on winglet $D_{i_{w.wl}}$.

(c) Drag due to winglet on winglet $D_{i_{w\ell,w\ell}}$.

(d) Drag due to winglet on wing $D_{i_{w\ell,w}}$.
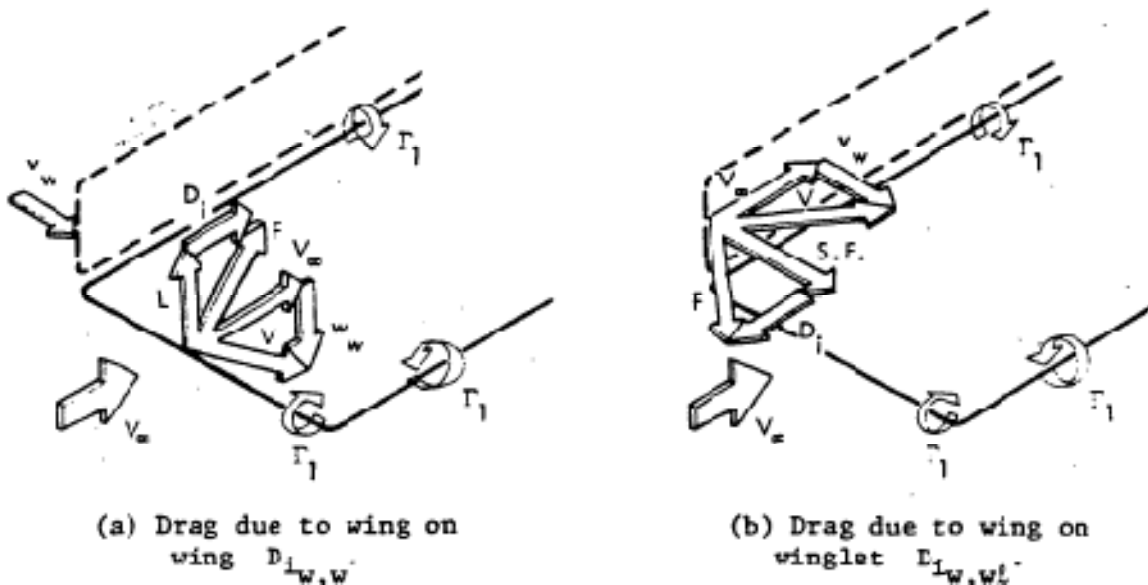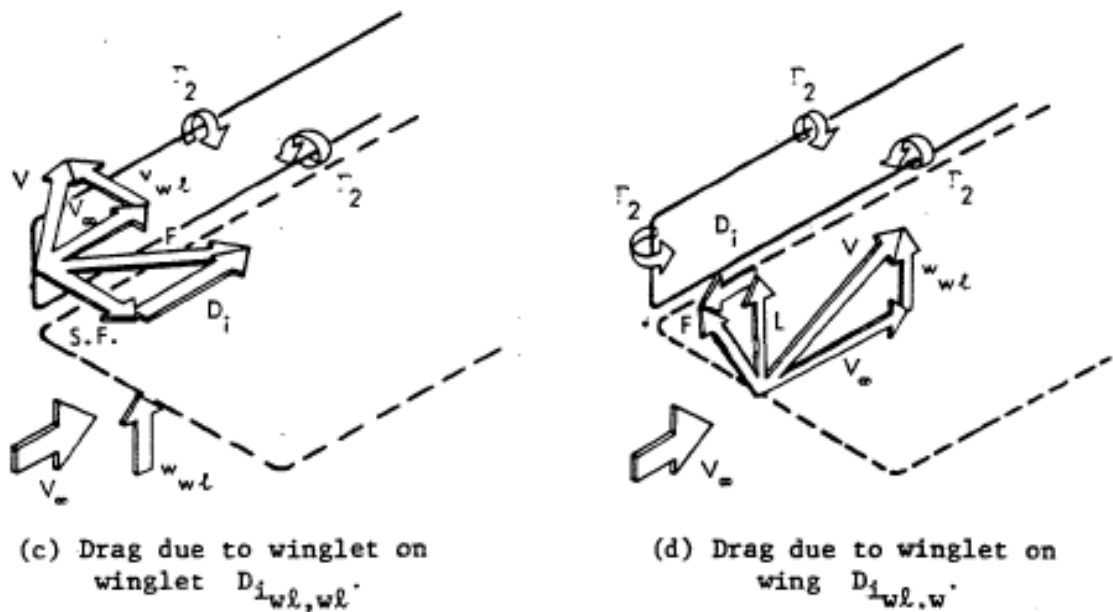
Figure 2.7 - Sources of induced drag for a wing-winglet configuration (Gall, 1984)

In figure 2.7d it can be seen that this upwash rotates the resultant wing force vector forward. This produces an additional lift force on the wing as well as a negative drag component.

Figure 2.8 below summarizes all the induced velocities. Such that the minimum induced drag velocity normal to the winglet must be zero. This happens when the sidewash produced on the winglet by the wing exactly cancels the sidewash produced by the winglet on itself. In other words, the induced angle of attack of the winglet is zero. The induced drag of the wing is also minimized by the presence of a winglet since the winglet causes a reduction in the net downwash at the wing; hence, the induced angle of attack is reduced. Also, the winglets allow the wing to be loaded more heavily towards the tips, which of course results in a more efficient wing.

OPTIMUM SIDE LOAD
FOR VERTICAL SURFACE

$v_{TOTAL} = v_{w\ell, w\ell} + v_{w, w\ell}$

$v_{TOTAL} = 0$

OPTIMUM VERTICAL LOAD FOR
HORIZONTAL SURFACE

$w_{TOTAL} = w_{w\ell, w} + w_{w, w}$

$w_{TOTAL} = CONSTANT$
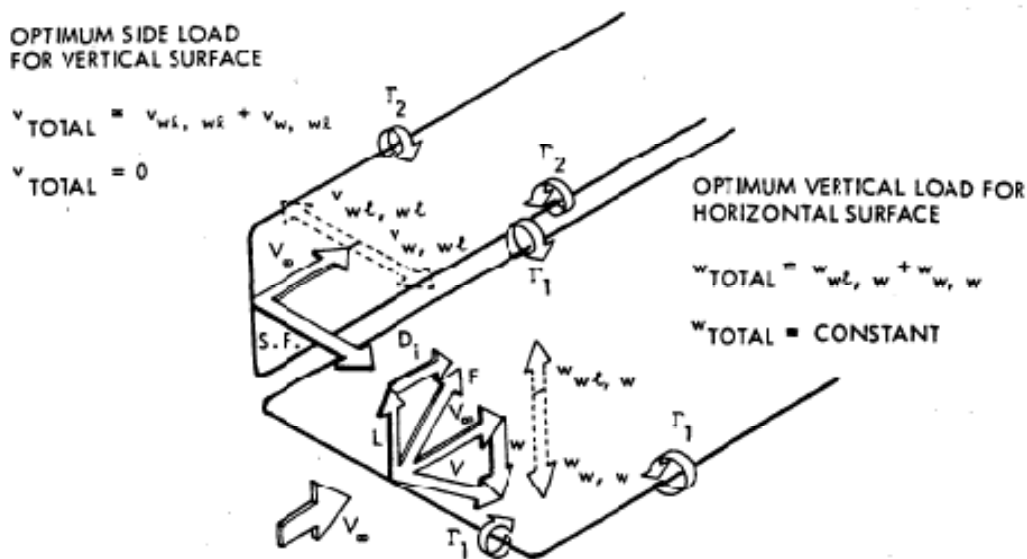
Figure 2.8 - Combined sources of induced drag for wing-winglet configuration (Gall, 1984)

As summarized by Kroo:

> *"Optimally-loaded winglets thus reduce induced drag by lowering the average downwash on the wing, not by providing a thrust component"* (Kroo I. , 2006)

2.8 Recent Research

Research on *"open"* nonplanar configurations, for example winglet and biplane designs has been intensively pursued over the past century as compared to the *"closed"* systems. For example the work done by (Whitcomb, 1976) proved to be a major milestone on application of winglets for induced drag reduction on commercial aviation aircrafts.

As this task is more focused on *"closed"* systems, thus the main research review will be predominantly carried on such systems. The initial work on closed systems mainly includes ring wings (Terry, 1964), joined-wings (Wolkovitch, 1986) and box-wings (Miranda, 1972).

The initial investigators were more intrigued by the structural advantages which can be attained by a closed system design. According to Wolkovitch (Wolkovitch, 1986) a 24% lighter aircraft may be realized by employing the methods and techniques of joined wing design. A joined wing can be described as two wings joined together at or near the tips. Similarly, the box-wing design study by Miranda covers structural benefits of such a design along with a potential decrease in induced drag. Subsonic and supersonic concepts of box-wings are proposed. It is also concluded in this report that box-wing configuration will

produce lesser wave drag or compressibility drag during the transonic speeds than a monoplane.

Over the past two decades, Professor Ilaan Kroo and his colleagues at the Stanford University have carried out detail research on various nonplanar concepts. Several concepts have originated from this design group which include C-wings (McMasters J, 1998) and a SWIFT sailplane (Kroo I. , 2000). The C-wing is an extension of box-wing concept in which a fixed circulation is added to the system so that the lower wing carries the entire lift and the upper wing carries none. The lift and vortex drag are unchanged (Kroo I. , 2005). A blended wing body having C-wing style tips is shown in figure 2.9 below.
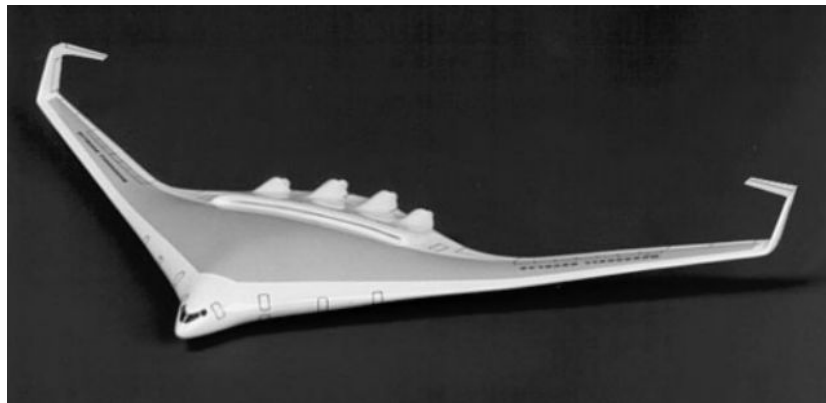
Figure 2.9 - Blended-wing-body concept with C-wing configuration for enhanced stability and control (Kroo I. , 2005)

A closed form solution of Prandtl's problem was given in 1999 by (Frediani A., 1999), confirming that Prandtl's approximate results were substantially correct for the wing gaps of interest. It was concluded that in the Best Wing System or box-wing, the lift distribution on the horizontal wings results from the superposition of a constant and an elliptical loading and, over the vertical wings, is butterfly shaped. Results are shown below in figure 2.10 (Frediani A, 2003)
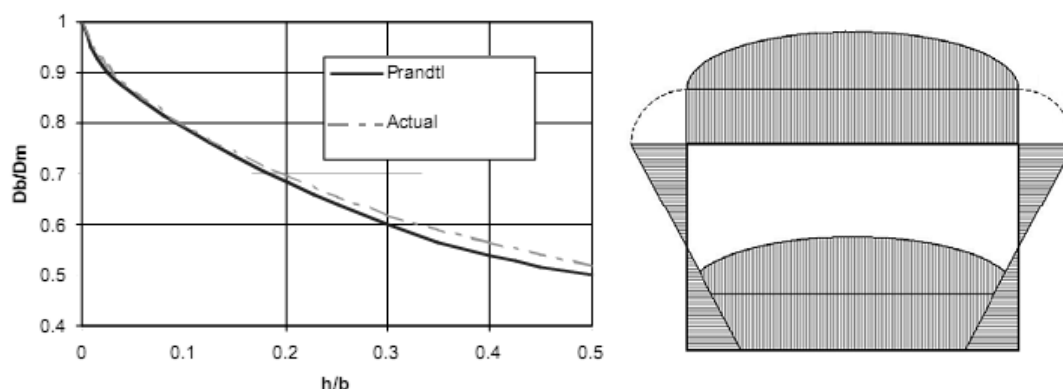
Figure 2.10 - Comparison between Frediani's and Prandtl's solution (Left). Lift distribution for box-wing (Right)

13

Sighting the potential benefits out of box-wing design, Frediani has recently worked on several aspects of this design. A complete design study has been carried out on a 250 PAX commercial variant of a box-wing design as shown in figure below.
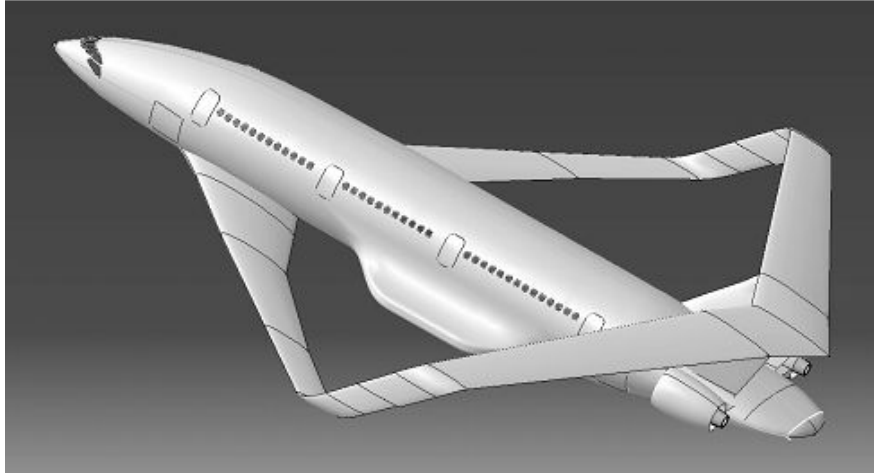
Figure 2.11 - Parametric view of preliminary study for a 250 PAX box-wing aircraft (Frediani A, 2005)

Frediani is currently the main researcher who is devotedly working on a box-wing concept and has written many technical papers. However his published work doesn't contain much detail about the procedure of the analysis carried out by him. Also he doesn't mention any of the problems he faced and solved while studying this design. Most of the research documents mainly contain the description of general benefits of box-wing and graphical representations of his work.

2.9 Conclusion

After this literature study it can be concluded that new concepts are needed to take aviation industry successfully into the 21st century. As concluded by Torenbeeck:

> *"The presently dominant configuration can no longer be improved, making the end of progress; if so, why the major manufacturers not (yet) apply them?"* (Torenbeeck, 2005)

By observing the work already accomplished by various researchers around the world it can be concluded that nonplanar configurations do have the potential to lead the aviation industry in future. At the same time, it can be seen that nonplanar configurations are different from conventional designs in-terms of aerodynamic and structural requirements needed to operate them successfully. Thus the design procedure required for constructing a successful nonplanar aircraft would be different from existing conventional aircrafts.

As far as box-wing is concerned, it is reducing drag by two techniques: winglets increase the span efficiency and dividing the single wing into wings having double or slightly less aspect ratios (depending on structural constraints) which improves the induced drag according to the basic aerodynamic theory. The box-wing design seems to have the potential to prove beneficial in both aerodynamics and structural domains, thus in-depth analysis of this configuration should be carried to truly understand the limitations of this design.

3 Problem Statement

As nonplanar configurations have fundamentally different design variables from conventional designs, the design approach for the following work is to first outline the basics of box-wing design and elaborates its design drivers. The goal is to investigate possible design issues of box-wing configurations. At this preliminary stage of analysis, low fidelity aerodynamic codes can be used to explore the variation of these design drivers. Further on, some higher order method can be used for example: Euler CFD method, to validate the results from lower order methods and carry out further investigations of box-wing design.

3.1 Box-Wing Geometery

In the following chapters, different geometrical aspects of box-wing will be discussed in detail. Thus it is important here to highlight and point out these fundamental geometrical aspects shown in figure 3.1.
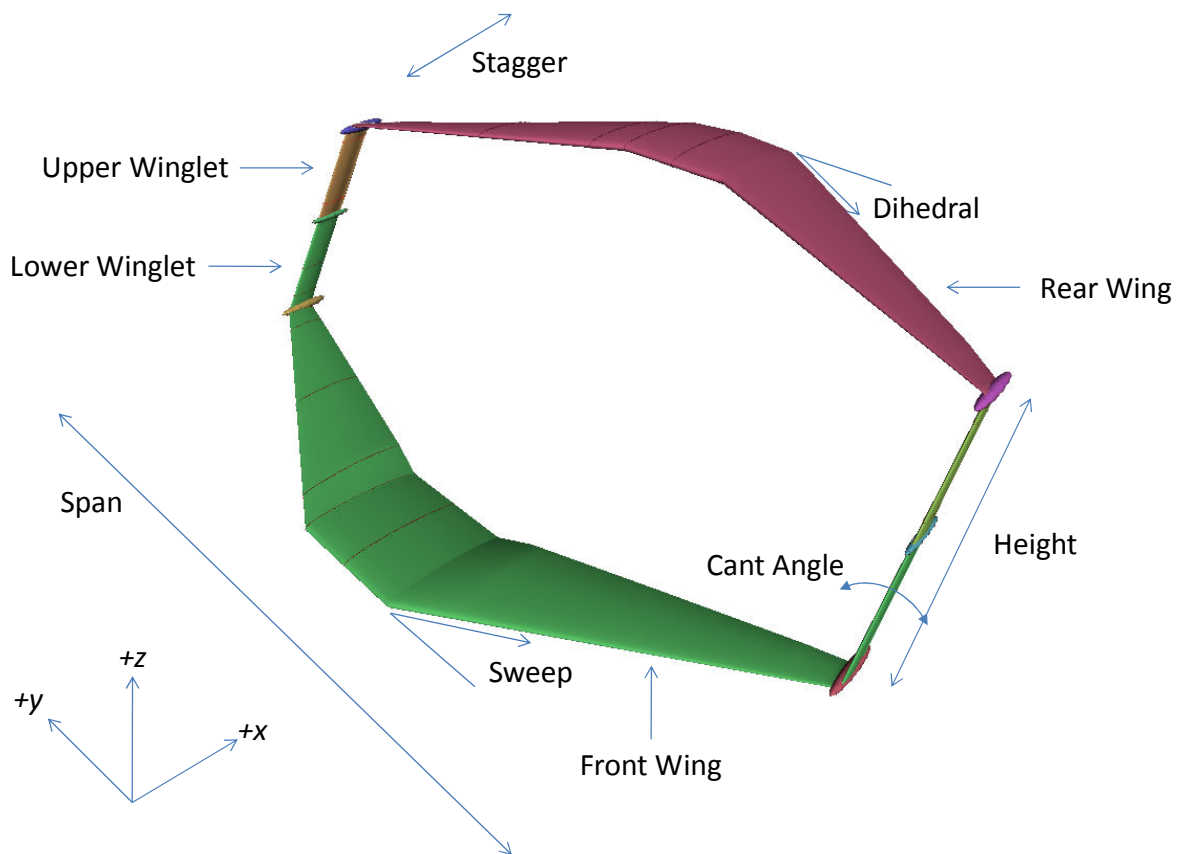
Figure 3.1 - Box-Wing geometry

4 Analysis with Vortex Lattice Methods

This chapter starts off with a brief introduction to vortex lattice methods (VLM). Then it introduces the different VLM codes used in this particular work.

A short summary and experience with Tornado is included. Afterwards analysis of box-wing using IDRAG is presented along with lattice convergence studies. Development and results of a canonical genetic algorithm are also included. A base model for box-wing is chosen based on the Airbus A320. Span loading for minimum induced drag is obtained. LAMDES code is utilized to determine the twist needed to maintain this required span loading. In the end, this chapter is concluded by a discussion on using VLM codes for preliminary design studies and potential improvements.

4.1 Introduction to Vortex Lattice Methods

Vortex lattice methods are much like finite-element methods in which the aircraft surface is represented by different planforms. Each planform is subdivided into a finite number of elemental panels, on which classical equations and theorems are applied for computation of the aerodynamic forces. These panels extend over the entire aircraft lifting surface both in spanwise and chordwise directions. Such methods are used in conceptual aircraft design studies and in aerodynamic investigations in general and have proven to be reasonably accurate and time efficient (Tomas, 2000). Primary outputs for the vortex lattice methods include lift, moments, induced drag, spanwise load distribution and wing efficiency factors.

Main assumptions made in VLM analysis are steady, irrotational, inviscid, incompressible and attached flow. Therefore, when analyzing lifting surfaces these codes can be only used in the subsonic speed range and assuming the surfaces are at low angles of attack. Such that the aerodynamic behavior is linear and the lifting surfaces are flying at well below the stall angle of attack. For preliminary design work, the Prandtl-Glauert correction is normally used to evaluate forces in compressible flows (Mach No. > 0.3).

For solution of flow properties over each individual panel a bound horseshoe vortex is imposed as shown in figure 4.1. Each bound vortex starts from infinity, arrives at its designated panel and crosses it at the quarter chord line and then returns to infinity forming the wake. Similarly at the three-quarter chord point a corresponding control point is located also shown in figure 4.1 below. Every control point on each panel satisfies a boundary condition of a no-cross flow through that panel (DeYoung, 1976). The flow field from all the vortices creates a downwash on the panel.

17

Further, the Biot-Savart Law is applied to calculate the induced velocity at the control point of a particular panel under the influence of all other panels. Using the Kutta-Joukowski Theorem (Eq-3.1), the force acting on every individual panel is calculated (Tomas, 2000) through.

$$\bar{F} = \rho(\bar{V}_{ind} \times \bar{\Gamma}).l$$

(4.1)

Where; $\bar{F}$ = Force, ρ = Density, $\bar{V}_{ind}$ = Induced velocity vector, $\bar{\Gamma}$ = Vortex strength and l = Length of vortex crossing the panel
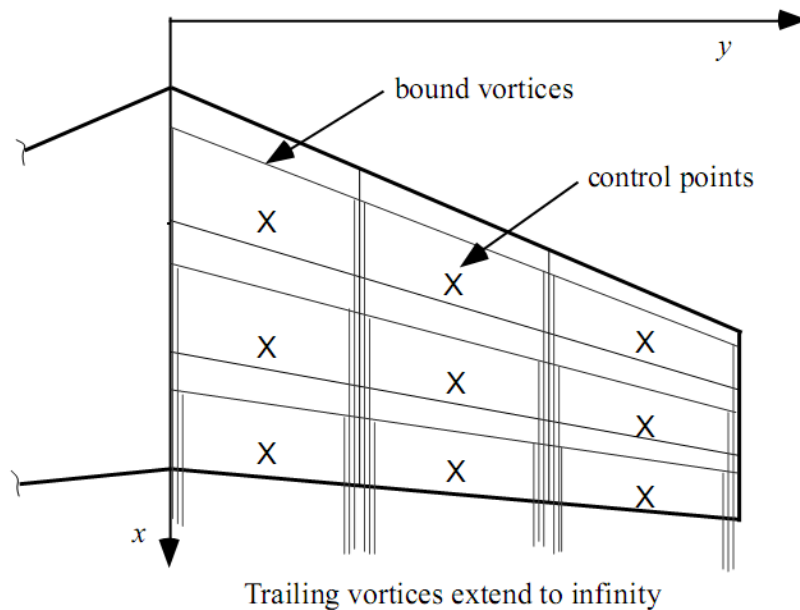
Figure 4.1 - The horseshoe vortex layout for a vortex lattice method (Mason, 1995)

Equations from all of panels form a system of linear equations which can be solved in matrix form using a computer. Eventually, all the forces are integrated to compute the resultant three dimensional force vectors on the surface.

4.2 Tornado VLM

Tornado is a vortex lattice method programmed by Tomas Melin as part of his master thesis at KTH Stockholm (Tomas, 2000). Over the time the code has matured and has been steadily updated and enhanced. It has also been compared with similar VLM and panel methods and has been found reliable (Tomas, 2000). The code is provided under the GNU-General Public License and can thus be altered and modified without the permission of the author.

Tornado is based on MATLAB® environment thus it is easily modifiable. The code supports any number of lifting surfaces arranged in any arbitrary fashion. Main outputs include lift,

18

span loading, coefficient of lift (*Cl*) distribution along span, stability derivatives and induced drag prediction.

Seeing all these benefits Tornado was first selected as the prime VLM software for this task.

4.3 Analysis with Tornado VLM

As mentioned earlier for a box-wing design the span loading is very important and has to be a combination of a constant and an elliptical loading on main wings for obtaining minimum induced drag. To first comply with this basic requirement, Tornado's output was investigated. It was found that Tornado assumes the first defined surface to be as the main wing. Resultantly it only plots the span loading and *Cl* distribution for the first main wing. The code was altered and a plot of span loading for the second surface (2nd wing) was included along with a reference plot of elliptical lift distribution. Further some changes in the code were made to lock the reference values to non-dimensional the induced drag values for multiple wing configurations.

Preliminary investigations were carried out to see the feasibility of Tornado code for nonplanar geometries. Analysis was started by first analyzing known configurations. Three configurations of nonplanar design were modeled these included, wing with a winglet, biplane and box-wing design. All three were designed according to height to span ratio of 0.2 so that there results can be compared with existing values in literature. Tornado's results were found to be closely resembling the expected values from literature ((Kroo I. , 2005) and (Grasmeyer, 1997)) as shown in table 4.1.

Table 4.1 - Span efficiency computed with Tornado and comparison with other theoretical studies

Test Case	Span Efficiency Values		
	Kroo	Grasmeyer - IDRAG	Tornado
Wing-Winglet	1.41	1.453	1.1423
Biplane	1.36	1.358	1.3992
Box-Wing	1.46	1.484	1.4781

Above analysis was carried out by constructing wings with a taper ratio of 0.45 and having no sweep. By doing so the lift distribution or span loading is found to be close to elliptical (Raymer, 1992). The box-wing and biplane configurations are analyzed without any stagger having height to span ration of 0.2.

As results from Tornado were found satisfactory further analysis on the biplane geometry was carried out. The biplane was chosen because at that moment the Tornado code was only

plotting lift distributions for two main wings and plots of lift distribution for winglets were not implemented yet. As the biplane wings were staggered, it was found that the span efficiencies decreased significantly and induced drag increased. Plots for staggered configuration were created and showed that both wings have different loading on them. To rectify this problem, wings now have to be twisted to obtain again a similar and an elliptical lift distribution. These plots are included as part of Appendix A. At this point, several attempts were made by twisting individual wings but the right combination was not found as twisting one wing influences the second wing in a different way and this iterative procedure was not bearing any good results. Secondly, the final analysis was supposed to have a design variable of sweep for main wings. When wings are swept the angle of attack changes along the span and finding the right twist for analysis was seen as a major problem.

At this moment it was decided to replace Tornado with a more suitable VLM code which can more efficiently capture nonplanar designs. Although the lessons learned at this point were important that the studies on nonplanar designs should be taken with extreme care even when using such low fidelity codes. The results differ a lot when the basic requirement (appropriate span load distribution) behind the nonplanar concept is not fulfilled. This can result in wrong analysis and the researcher can be misled. For example, after staggering the wings and not correcting the twist to achieve the right load distribution, the researcher can conclude that positive or negative stagger is influencing span efficiencies. In reality, the circulation on both wings has changed and is not similar anymore. It must be corrected to achieve the similar span efficiencies again as for the wings without stagger.

4.4 IDRAG VLM

IDRAG is a code written by Joel Grasmeyer at Virginia Polytechnic Institute and State University. This program is specially created to calculate the induced drag of nonplanar lifting surfaces. It has both design and analysis capabilities. This means that either the spanload required to obtain the minimum induced drag can be found, or if a spanload is included in the input than it can find the induced drag for the given set of surfaces. The program also calculates the span efficiency factor *e* (Grasmeyer, 1997).

Comparing with Tornado, IDRAG utilizes a different scheme for calculating induced drag. In IDRAG computation of all forces is done in the Trefftz plane, which is a plane defined in the wake of the aircraft at infinity such that it is perpendicular to the wake. By using the Trefftz plane, the induced drag calculations are independent of the *x-coordinate, which effectively reduces the 3-dimensional problem to a set of 2-dimensional equations* (Grasmeyer, 1997).

This technique is based on Munk's theorem and for detail explanation (Gall, 1984) is recommended.

As this code was specifically written, compared and validated with the results of other researchers for nonplanar configurations. It is thus perfectly suited to the requirement of this project.

4.5 Analysis with IDRAG VLM

IDRAG uses a text input file in which corner points of the required geometry are defined. Several test cases were run to get use to the different features of the code. Also some given example in the IDRAG manual were solved and plotted to see that code was working appropriately.

4.5.1 Selecting a Base Design

A typical IDRAG input file contains different reference values along with information regarding the geometry of the surfaces to be analyzed. To fix these reference variables like design lift coefficient, operating Mach number and other reference values, an Airbus A320 was chosen as the baseline aircraft. Typical values used during the analysis are shown in table 4.2 below (Jane's all the world aircraft, 2009). Some of the values were computed based on available data, for example coefficient of lift was computed by using maximum take-off weight and cruise conditions.

Table 4.2 - Reference data from A320 for IDRAG analysis

Specification	Notation	Value	Units
Wing Reference Area	S_{ref}	122.4	m^2
Span	b	34.1	m
Aspect Ratio	AR	9.5	-
Wing Quarter Chord Sweep	$\Lambda_{c/4}$	25	°
Taper Ratio	λ	0.24	-
Root Chord	c_r	6.10	m
Mean Aerodynamic Chord	MAC	4.29	m
Weight – Empty	W_e	42100	Kg
Weight – Maximum take-off	W_{MTOW}	77000	Kg

21

Cruise Mach No.	M_{cr}	0.78	-
Cruise Altitude		11280	m
Cruise Lift Coefficient	$C_{L_{cr}}$	0.67	-

4.5.2 Convergence Study

As vortex lattice methods perform calculations on individual panels to compute the resultant forces acting on a given geometry, the number of panels defined plays an important role in the accuracy of the solution. The panel number influences the results and if not defined adequately may not capture the complete effect of the set of surfaces. At the same time, it was intended to build an optimization algorithm around the IDRAG VLM code. For such an algorithm repetitive analysis is carried out and run-time performance is important. If the number of panels defined are too many than the code will take a longer time to evaluate geometry. Resultantly the complete process would be time consuming.

Keeping all these issues in mind, a panel number variation study was carried out, to find minimum number of panels required to analyze different geometries adequately. During this procedure, it was important that the results shouldn't vary on the basis of inadequate number of panels rather than variation in geometry. It was found that the minimum number of panels which gave reasonable accuracy were 30 panels for each main wing and 10 panels for winglets (combined).

4.5.3 Defining Design Variables

If a box-wing configuration is studied carefully several design features are present which need to be investigated. The main features are, height to span ratio between the two wings of the box-wing design and the aspect ratio for main wings. Similarly, the taper ratio for both wings can be studied and dihedral or anhedral effect can be investigated too. By keeping the Munk's theorem in mind, sweep and stagger should have no effect on the box-wing design if optimum span distribution is maintained. Nevertheless, it would be important to vary both of these parameters to see whether the code is capturing the box-wing design features completely or not.

Some of the design features can be neglected by seeing the basic requirements of box-wing design. As stated earlier, a box-wing should have an equal distribution of lift among the two main wings. Thus this restricts the studies from looking into unequal main wings for minimum induced drag condition. Similarly, different aspect ratios for individual wings don't

make sense as both wings are having identical wing area and should have a maximum possible aspect ratio to achieve minimum induced drag (with structural constraints).

Other aspects for example airfoil selection and polyhedral wing shapes can be investigated too. As far as the airfoil selection is concerned, for this preliminary analysis it is not studied as the IDRAG code doesn't take into account an airfoil selection. Similarly, polyhedral feature is not directly studied but can be inferred from the study of dihedral and anhedral cases.

4.5.4 Results from Design Variables Variation

Different results for several design variables are shown and discussed below. As a range of values were taken into account for every design variable to capture the complete influence of that variable on the box-wing design. Thus, a MATLAB® based script was created which generated the input file for every individual case. The IDRAG input file requires corner points for defining the geometry of different surfaces. Based on the main design variables a global set of parameters similar to design variables were passed on to this script which in return automatically defined a geometry based on input values. This script is called *IDRAG_in.m* and is included in Appendix C. It automatically calls IDRAG by using a subscript made in AutoIt® and returns the value of coefficient of induced drag and span efficiency factor from the IDRAG output file.

4.5.4.1 Validation of Munk Theorem

Several computation runs of individual values of stagger and sweep were made using the *IDRAG_in.m* file running on the IDRAG code. Positive stagger was varied from zero to five multiples of *MAC*. Similarly, negative stagger was varied from zero to negative five multiples of *MAC*. For sweep both wings were independently varied from -45° to +45° quarter chord angles. In all of these variations span efficiency factor and induced drag remained constant.

Thus it can be concluded that the IDRAG code is computing the geometries correctly and is finding the similar optimum span loading for every run. These results validate the Munk's stagger theorem: box-wing design is independent of sweep and stagger if the correct span loading is maintained.

This has important consequences; if we can achieve similar drag reduction independent of sweep, transonic wings can be designed for a box-wing configuration. Wing sweep is an important factor by which the compressibility drag can be reduced during transonic speeds. It also allows the use of higher thickness to chord ratio airfoils which result in lighter structure (Obert, 2009).

Stagger has similar advantages; by introducing stagger the interference of supersonic flow among the two main wings can be reduced at transonic speed. At the same time, increased stagger can positively influence the stability of the box-wing design.

4.5.4.2 Height to Span Ratio Variation

Height to span ratio variation is the most important design variable for a box-wing aircraft. Here the general trend can be understood as that when a single wing is divided into two wings having the same total area and span as the original wing, maximum induced drag reduction is achieved (Raymer, 1992). In other words aspect ratio has been doubled and as per basic aerodynamics an increase in aspect ratio reduces the in induced drag.

It is important to understand the relationship of aspect ratio and induced drag reduction of box-wing aircraft. If the full advantage of a box-wing aircraft is to be taken than the span of the two main wings for box-wing aircraft should be the same as that of a reference monoplane. In such condition minimum induced drag reduction is possible as shown in figure 4.2 *(AR = 19)*. The reduction increases as the gap is increased because the mutual interference factor between the two main wings is decreasing.

If the aspect ratio of the reference aircraft is maintained for the box-wing (AR = 9.5), then the box-wing aircraft will have even higher induced drag then the reference monoplane aircraft. Figure 4.2 shows (green straight line) the minimum induced drag attained by the A320 reference aircraft during its cruise phase (span efficiency factor of unity). With a decrease in aspect ratio the potential advantage of the box-wing aircraft subsides. For an intermediate aspect ratio this means; for example that a box-wing aircraft having an aspect ratio of 13 has to have a greater gap than a box-wing aircraft with an aspect ratio of 19 to significantly reduce the induced drag.

For a practical design, it is important here to take into account the effect of the lower chord value by choosing high aspect ratios as this will result in problems associated with low Reynolds number effects. Also structural design will get intensified as aspect ratio is increased.
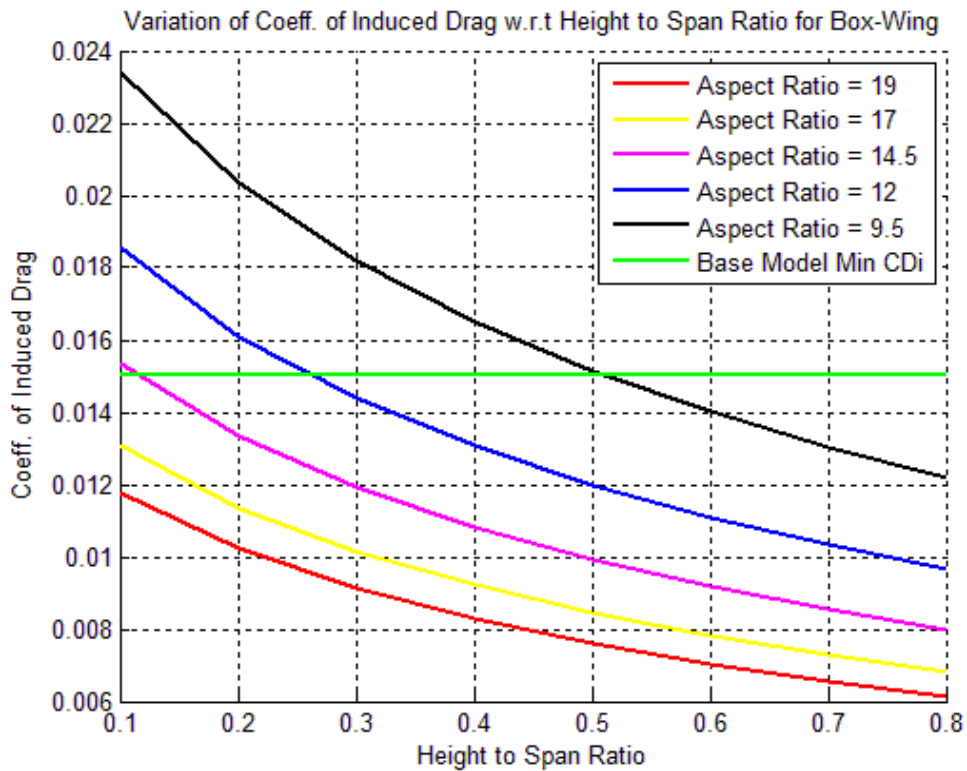
Figure 4.2 - Variation of induced drag with height to span ratio

4.5.4.3 Dihedral Variation

Furthermore, different dihedral angles for individual main wings have been investigated (figure 4.3). The variation was conducted between 0° to 10° dihedral for the lower wing and of the 0° to -10° of the anhedral for the upper wing. It can be seen that the maximum reduction is possible when choosing zero dihedral and anhedral angles for both wings. Further it can be foreseen that induced drag can even be more reduced by increasing the dihedral of upper main wing and anhedral of lower wing thus making the wing tips move further apart vertically. This will however have a negative influence on the stability of the aircraft.

Once again it can be concluded that the general trend of effects of the dihedral angle are shown here, but the actual value being used in a box-wing design will also be dependent on structural and stability aspects of choosing the dihedral or anhedral angles.

25
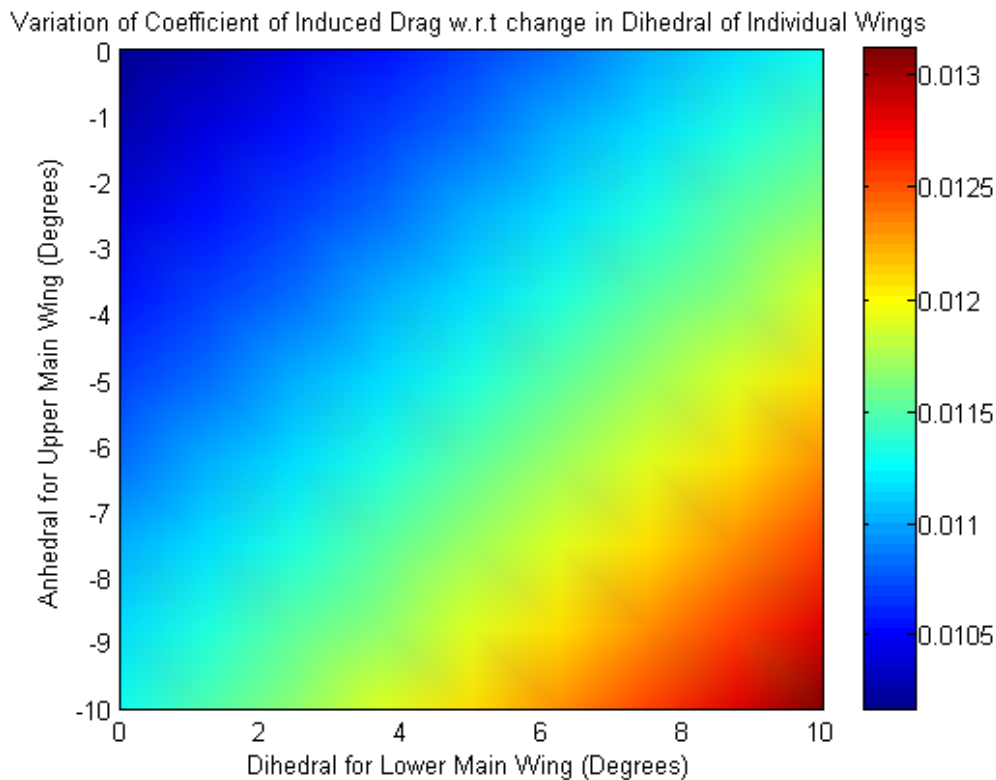
Figure 4.3 - Variation of coefficient of induced drag with change in dihedral for individual wings

4.5.4.4 Taper Ratio Variation

The taper ratio was independently varied for each main wing from 0.1 to 1, 1 representing an untappered wing, at an interval of 0.18. Several runs were made to assure that code was working fine. For every run it was concluded that for a box-wing, the taper ratio selection has no effect on its aerodynamic design. This can be explained as; the IDRAG code for every chosen taper ratio value readjusts the span loading so that the induced drag is minimised. Or in other words, any taper ratio can be chosen as long as the twist of the wing takes account of the required span loading.

Again the taper ratio selection is a function of aerodynamics as well as structures. This solution was run with an inviscid solver and thus doesn't take into account the low Reynolds number effect on wing tips if the wing is highly tappered.

4.5.4.5 Cant Angle Variation

Cant angle is defined as the mounting angle of the winglet with respect to the main wing. If the winglet is mounted perpendicular to the wing the cant angle is 0°. It is negative when winglet is tilted towards the wing (inside) and positive for tilt direction away from the wing.

26

When it is positive, it is adding up to the total span of the wing. Thus it is expected to produce an induced drag reduction as effective span is increasing.

Figure 4.4 below shows the variation of cant angle for a box-wing configuration. This cant variation was computed for a specific aspect ratio design but the variation is the same for any chosen span or aspect ratio. The desired aspect ratio (close to 19) for a box-wing design would probably not result in a good structural design. Thus, by choosing a lower aspect ratio a good design option can be achieved by positive cant angle winglets.
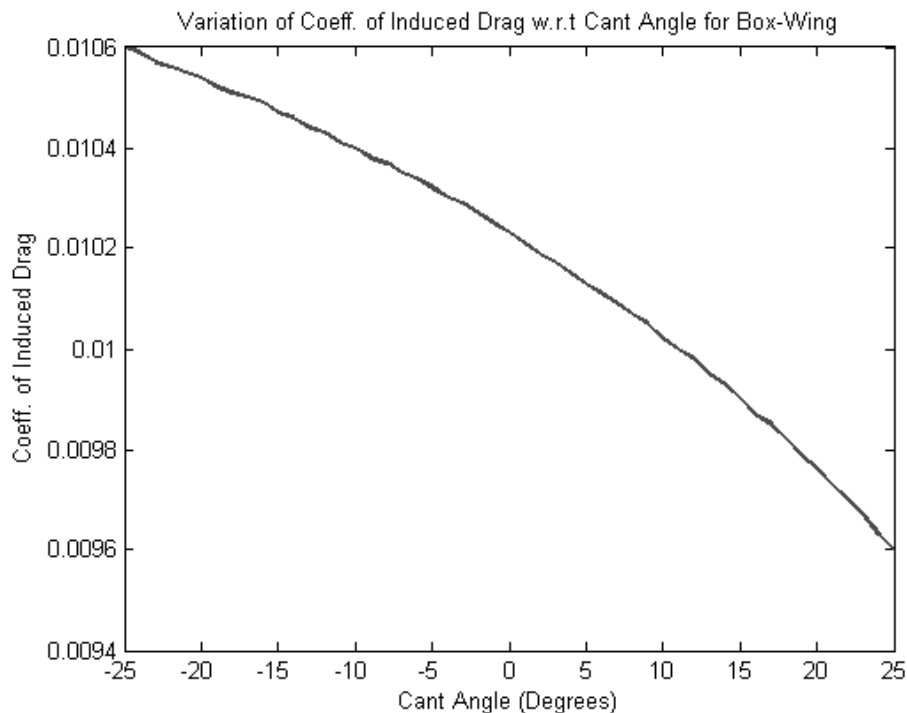
Figure 4.4 - Variation of coefficient of induced drag with winglet cant angle

4.6 Canonical Genetic Algorithm (CGA)

When studying the variation of design parameter individually there is a chance that the global maximum of the design is not attained. With individual parameter sweeps, local maxima can be located for every variable but this can't guarantee that these local maxima would also lead to a global maximum, when all of the variables are considered collectively. To accomplish this task an algorithm was developed based on principles of genetic evolutionary processes (Holland, 1975). With the help of Mike from Aero and using (Stuart & Peter, 2003) as reference the following work was accomplished. The code is included in Appendix D.

The algorithm starts off with the initialization of all design variables. Afterwards from the pool these design variables, random values are selected to form ten parents. This selection is

27

totally random and every value of any variable has equal chance of being selected for formation of any of the parents. However, for the values from design variables which are selected for one parent, then these values are not selected again for any other parent so that a more versatile group of parents can be formed.

```
Initialization of          Generating Initial
Parameters                 Population
                           Parents

                    Evaluating Span
                    Efficiencies

Max Iterations                          Crossover
Reached ?                               Children
                                        (Only for worst 5)

Print out                  Mutation
Best Individual            In Children
                           (Except best 3)
```
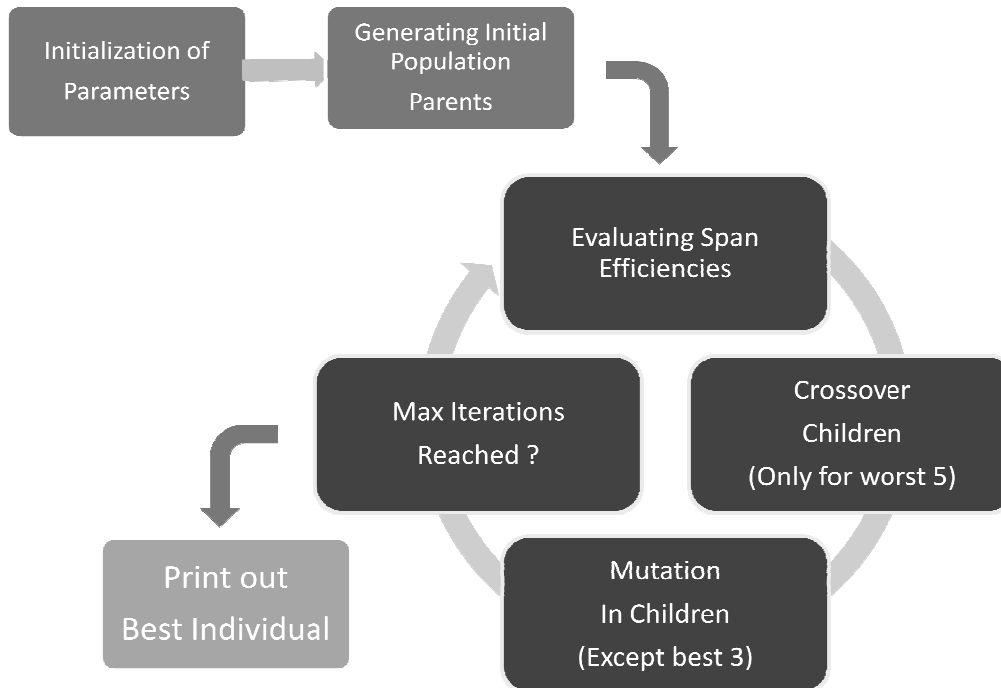
Figure 4.5 - Canonical genetic algorithm flow chart

After generation of ten parents, the program enters the optimization loop as shown in figure 4.5. Than IDRAG is called through the intermediate script *IDRAG_in.m* mentioned before. Span efficiencies are evaluated and are fed back to the optimization loop of the main code for every parent. Depending on span efficiencies parents are sorted out. Than the *best* five parents are saved separately while the lower five are sent for a crossover procedure.

Crossover is an important random operator in CGA and the function of crossover is to generate a new "child" from the selected "good" parents. All five good parents are used in this process to create new five sets of *children* to be evaluated again. All of the *bad* five parents are now replaced by these newly formed *children.*

At this point in the script, all of the values of variables being used in parents and new children are from the initial set of five good parents out of original ten parents. As the selection after initialization was made on random basis, it is less likely that the best combination of variables is among the first ten parents. Therefore after crossover, mutation is carried out. Mutation operates independently on the two old parents and new five children.

28

The three best parents are left out of this process so that during an optimization the good qualities of the best three parents are not lost due to a random mutation. Mutation acts randomly on these seven parents, and introduces fresh values of design variables into their data sets. In doing so, later on during optimization if any of the parents gets high span efficiency value it is moved to best three accordingly thus gradually solving for the best combination.

After the mutation is complete all of these parents are again sent to the *IDRAG_in.m* file through a loop and the complete process is repeated. This cycle continuous till a convergence is met or the allotted loop limit is expired. After that the design variables for the evaluated best case are printed along with convergence plots.
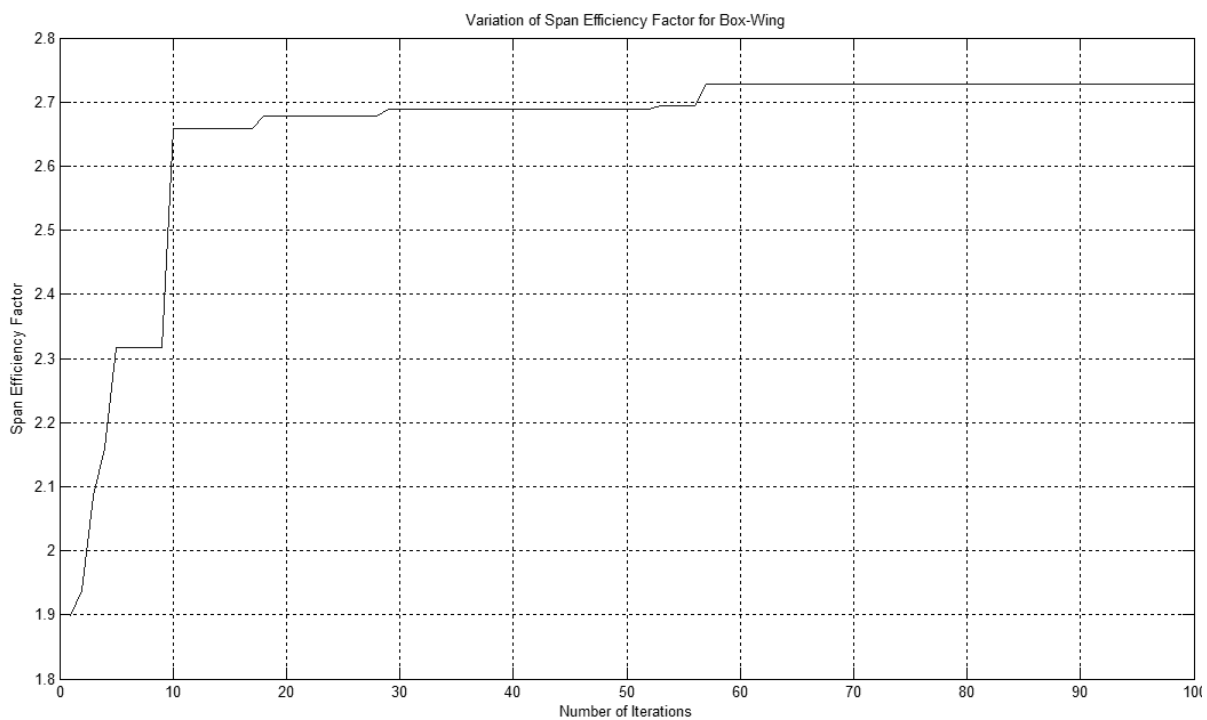
Figure 4.6 - Convergence plot of CGA

Several test cases were run and it was found that within hundred optimization cycles global maxima of the design variables could be evaluated. One of the test run convergence plot is shown in figure 4.6 above.

The results of this study using CGA, concludes that the global maximum is located at local maximums of each design variable. As for a purely aerodynamic analysis this result was expected but if this optimizer is coupled with a structural design evaluator (having weight constraints) than a more realistic final global maximum can be found using this code.

29

Based on the results of CGA and parameter variations, a box-wing configuration has been selected for further analysis. The chosen aspect ratio is 14.5 for individual main wings with height to span ratio of 0.3 as shown in figure 4.7. Although, this analysis would be of purely aerodynamic nature but yet, the chosen box-wing configuration has lesser span than reference aircraft (Reference Aircraft Span: 34.1m – Selected box-wing Span: 29.78m). The box-wing having reduced span can compensate for the additional structural weight added due to the presence of the winglets. Thus it can be concluded for analysis intent that the total weight of both configurations will remain same. The predicted coefficient of induced drag for these parameters is 0.01191 as compared to 0.01467 for the reference A320. This leads to an almost 20% reduction in induced drag. Here it should be noted that current civil transport aircraft do not fly at their optimum span loading values. Rather under influence of structural weight constraints the span loading is restricted to more of a triangular distribution rather than elliptical. As for elliptical load distribution, the lift centre is located at 42.4 % of span (outward as compared to triangular distribution) thus resulting in heavier wings. So the induced drag value selected here for the reference aircraft is actually less as compared to practical design. Thus, in reality this can result in even higher drag reduction if the box-wing design is, instead of the reference aircraft, following an elliptical load distribution.
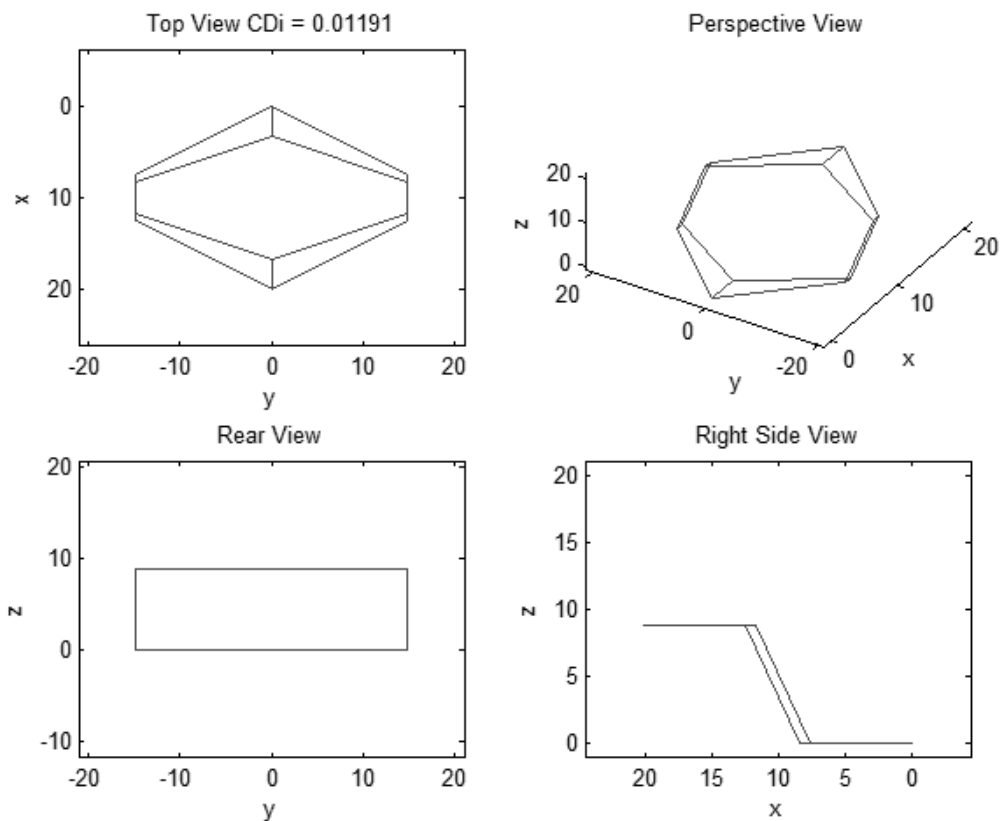
Figure 4.7 - Selected box-wing configuration for CFD study

For this initial analysis no dihedral was taken and main wings and winglets sweeps were chosen to be 25° which is the same as for the reference aircraft. Computed span loadings for the above configuration for minimum induced drag are shown in figure 4.8. It can be seen that front and rear wing have identical, combined elliptical and a constant lift distribution. Prandtl suggested only elliptical loading but in a more exact solution, Frediani suggested an elliptical distribution added to a constant distribution (Frediani A., 1999). The addition of constant distribution can be explained because of the presence of winglets. For optimally loaded wing-winglet combination such distributions are formed. For winglet sections, the optimum distribution is almost triangular as shown in figure 4.8.
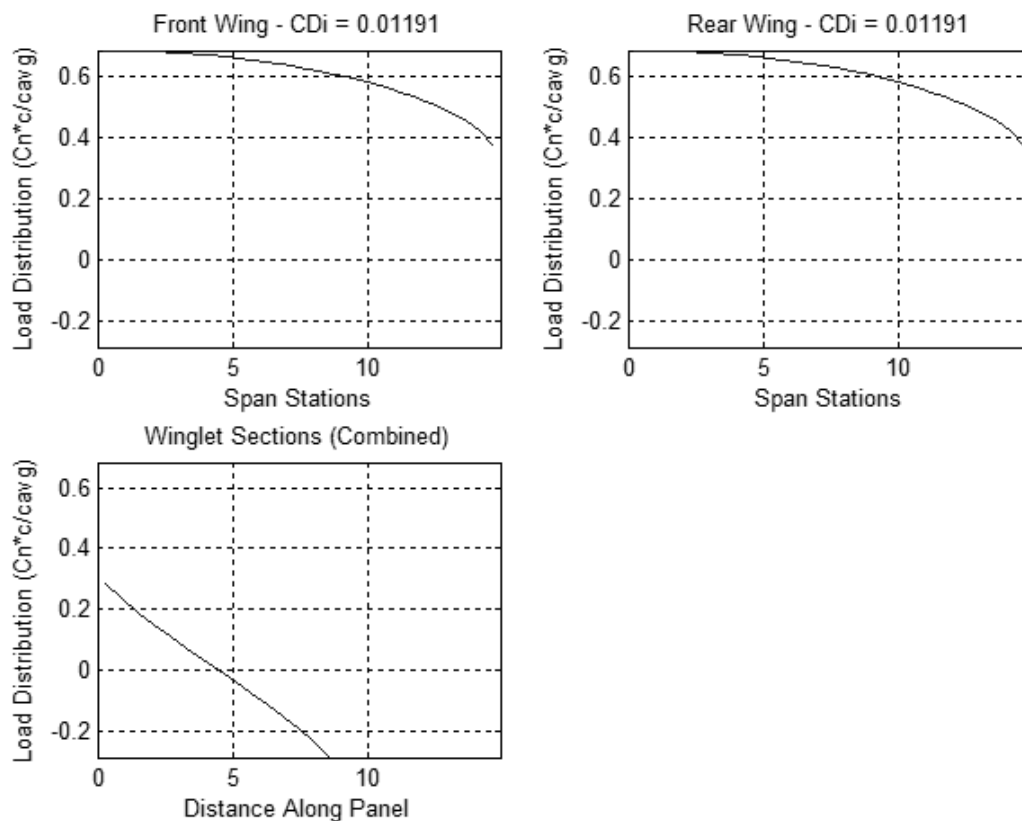
Figure 4.8 - Computed optimum span load distribution for box-wing aircraft

If above figure is more closely observed, the value for which the load distribution ends at wing tips and starts at the winglet root is not identical. This also agrees to the wing-winglet optimum distribution as can be found in (Kroo I. , 2006). For winglets, the lower winglet has side force generated inwards while for the upper winglets it's the other way around.

Using these optimum span loadings further work was accomplished with LAMDES code for computing the required twists to obtain these loads.

4.7 LAMDES VLM

LAMDES is a VLM optimization code and is made available by Dr. Mason from Virginia Polytechnic Institute and State University. This code can also handle nonplanar surfaces but is limited to only two surfaces. It can find the surface twist needed to attain the minimum induced and pressure drag values. It can also provide camber distribution along span and it can find minimum trim drag for moment constraints (Mason, 1995).

4.8 Analysis with LAMDES VLM

For this work, LAMDES was mainly used to calculate the twist required to maintain the span loading calculated by IDRAG. Initially, it was intended to model a complete box-wing in LAMDES such that the estimates from IDRAG can be re-confirmed. The code is limited to two surfaces, so the box-wing was to be modeled as two wing-winglet combinations. During the test runs, it came out that LAMDES is not able to comprehend the winglet surface completely. The twist distribution along span is only computed for the main wing and the winglet is left out. As for the box-wing configuration, winglets carry their own specific loadings. Thus it was decided to model each surface individually.
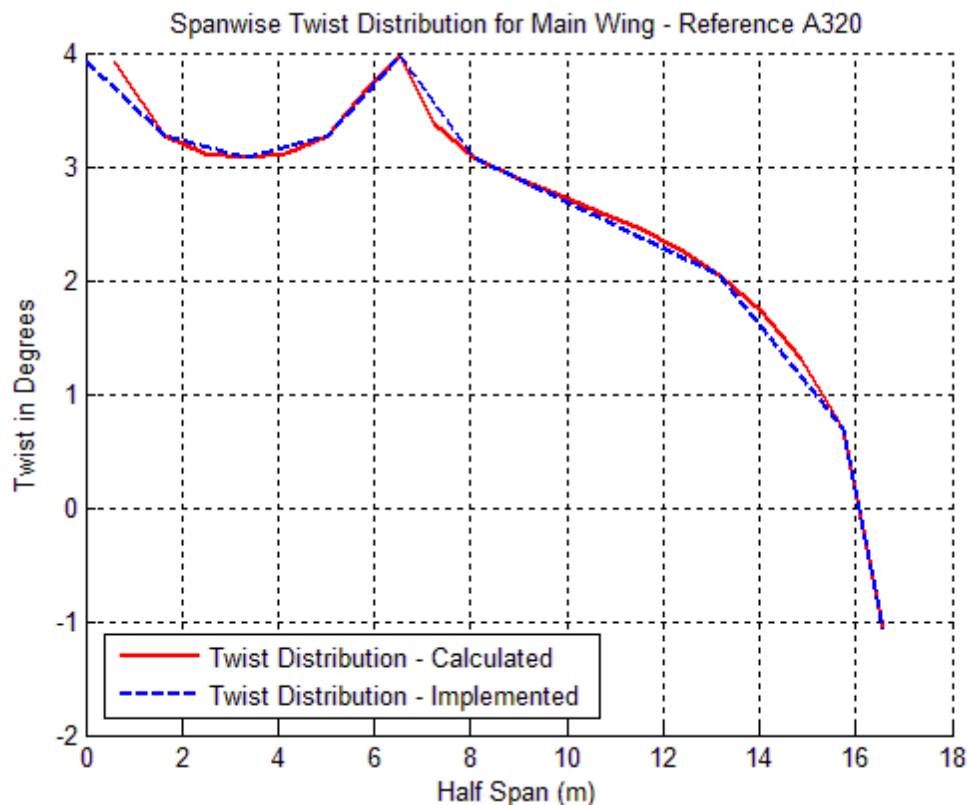
Figure 4.9 - Spanwise twist distribution for reference A320

32

Another limitation of the code was found to be that the code assumes a chordwise loading for NACA 6 series airfoil sections. Nevertheless, the code can be used for initial estimates on twist distribution for the transonic regime too (Andy, 2002).

The reference A320, a single surface configuration, was modeled completely in LAMDES. Figure 4.9 above shows the twist distribution along the span. Having a swept aft wing the twist distribution is following the theoretical trend and has been computed for elliptical span loading. The peak in the twist distribution occurs due to the sudden change of a chord station where the engine pylon is attached along with the main landing gears assembly. This peak was expected as for a sudden change in chord along span the twist rises up to compensate the loss of lift. As sudden spanwise changes in chord distort the 3-D flow and thus cause loss of lift. The dotted blue lines show the implemented twist of the later more detailed model of the reference wing.
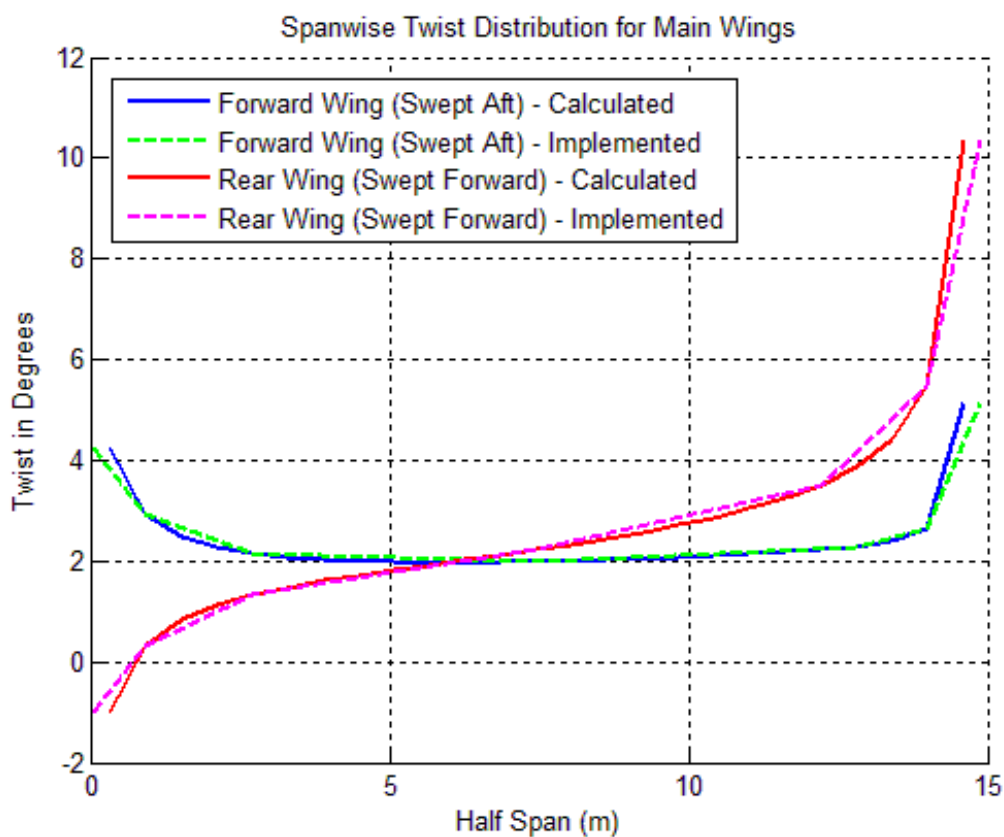
Figure 4.10 - Spanwise twist distribution for main wings of selected box-wing configuration

For box-wing calculations, the IDRAG span loading was imported into LAMDES file (with the limitations of not completely capturing the twist if winglets with LAMDES) and each surface was dealt individually. LAMDES was bound to utilize the given span loading and estimate the twist accordingly. Figure 4.10 shows the twist calculated for individual main

33

wings of the selected box-wing configuration. It can be seen that the twist distribution trend for a swept aft and swept forward surface is in accordance with the theory. The wings are heavily loaded towards the tip. Thus for a swept aft wing the twist distribution rises up again near its tip region. Similarly, for a swept forward wing out of basic aerodynamics the effective angle of attack increases along the span from tip to root. To maintain the high loading the tip is at high angle of attack and the root even goes down to negative. Here it should be kept in mind that the local chord distribution along the span is also affecting the amount of twist needed at a particular span station.

Furthermore, several span stations were selected along the span, values from these stations would be used to construct the 3-dimensional model of the box-wing for further analysis. For both wings, 6 span stations are being used to fully capture the twist along the span; this implemented twist is shown by the dotted lines above.
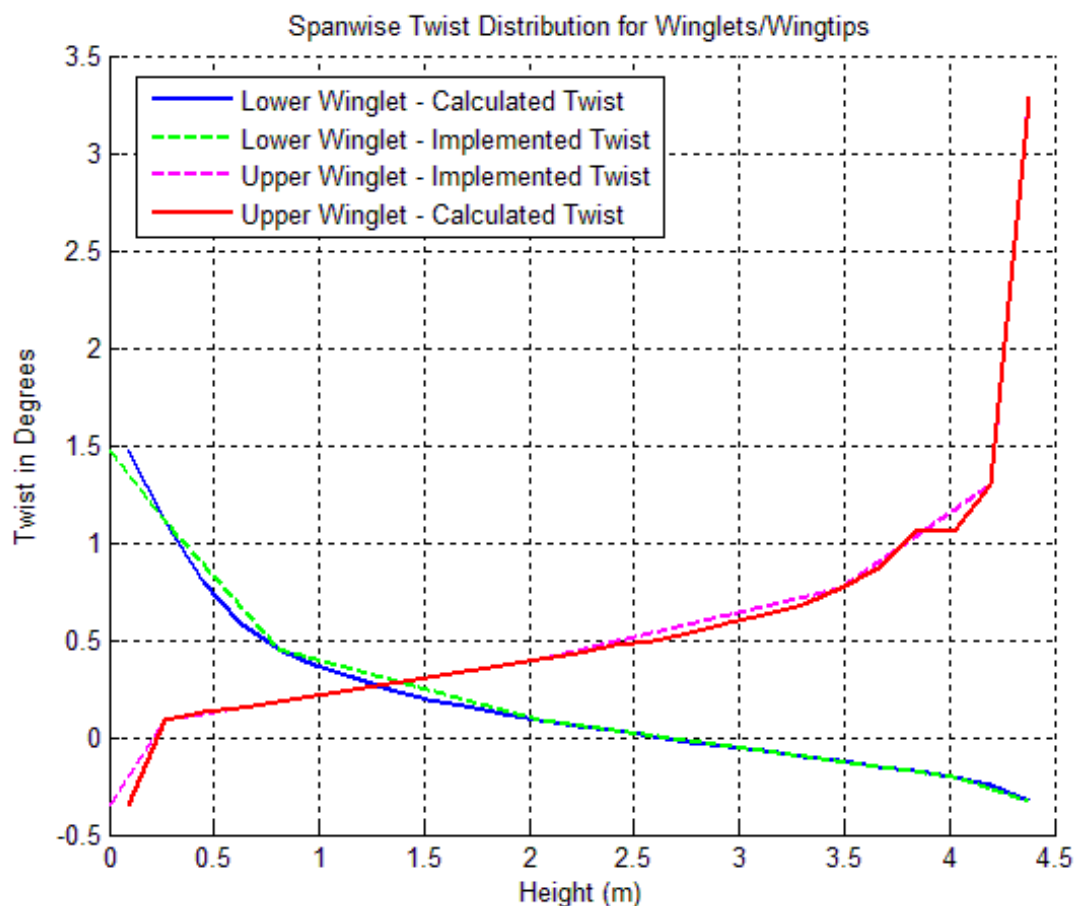
Figure 4.11 - Spanwise twist distribution for winglets of selected box-wing configuration

Similarly, each winglet section was modeled separately in LAMDES. The span loading was imported from IDRAG and implemented in the input file for LAMDES. The lower winglet

was modeled from root to tip as shown in figure 4.11. The upper winglet was modeled the other way around i.e. from tip to root. In the plot below, both winglets start from their lower span stations and move upward along their respective spans. Dotted lines show the span station selected of the model analyzed in more detail later on.

Here it should be noted that figure 4.11 shows the incidence angle need to maintain certain span loadings for individual winglet sections. Both winglets are loaded in different directions so the twist shown above should be used accordingly following the convention of loadings in a box-wing configuration.

4.9 Conclusion

The analysis with a vortex lattice code was completed. It has been found that VLM codes do capture the effects of nonplanar designs and thus can be used to further explore different aspects of such unusual designs.

The work accomplished in this section can be used to further investigate the box-wing design. It can help to identify key components in design and at the same time leave out the ones which are less important. Span loading obtained from IDRAG follow closely the predicted load distribution of previous investigators. The prediction of induced drag reduction can also be seen and the amount of reduction follows the same trend as earlier anticipated.

It can be concluded here that the work by VLM codes was following the right trends and thus a simple model can be generated by VLM codes for further aerodynamic investigations as shown in the next chapter.

At the same time, during performing the tasks in this section it was felt that a structural model of the system under investigation should be coupled with aerodynamic investigations especially with the CGA script. This can lead to a more realistic approach to the answer of the potential of induced drag reduction with cost of added weight upon the complete system. Similarly, keeping the stability issues in mind a simple stability model should be included to further increase the reliability of the analysis.

5 Analysis with Euler Code

This chapter starts off with an introduction to Euler methods used in the field of Computational Fluid Dynamics (CFD). Then SUMO® a rapid CAD generator specially designed for aeronautical applications is introduced and the work accomplished using this software is explained. Afterwards the Euler flow solver EDGE® is briefly described.

In the second part of this chapter the solutions carried out by the EDGE® solver are described. Results are outlined and possible limitations in the derived solutions are cited.

5.1 Introduction to Euler Method Codes

The Euler method or the Euler equations by definition neglect the viscous component of the 3-dimensional flow field. This results in inviscid flow having no effect of friction and thermal conduction (Anderson J. D., 1995). The three basic equations of fluid are given below in Euler form as:

Continuity Equation:

$$\frac{\partial \rho}{\partial t} + \nabla.(\rho \mathbf{V}) = 0$$

$$(5.1)$$

Momentum Equation:

$$\frac{\partial \rho \mathbf{V}}{\partial t} + \nabla.(\rho u \mathbf{V}) = -\nabla p$$

$$(5.2)$$

Energy Equation:

$$\frac{\partial E}{\partial t} + \nabla.(\mathbf{V}(E + p)) = 0$$

$$(5.3)$$

Where; ρ= Fluid mass density, $\mathbf{V}$= Fluid velocity vector, E= Total energy per unit volume, p=fluid pressure

The flow is unsteady and rotational in nature, but still capable of describing shock waves (compressibility effects) and fairly good in predicting lift. The drag prediction by choosing the Euler methods is limited to induced drag and compressibility drag. Nevertheless, this current work is oriented towards investigations of induced drag reductions thus choosing the Euler based solution is a suitable decision saving time and computational efforts.

The main advantage of Euler method is to estimate the lift coefficient and induced drag components of the three dimensional flow in considerably less time than complete Navier-Stokes equations. The surface boundary condition for an inviscid flow is that the normal velocity component has a zero value at the wall i.e., the velocity vector near the wall is tangent to the wall. As the boundary layer at the walls is not needed to be resolved, a coarser mesh can be adopted for the overall geometry by further reducing the computational time (Ferziger, 2002).

5.2 SUMO® (Rapid CAD)

To conduct an Euler solution for the selected box-wing configuration, a detailed geometrical model was required. This task was accomplished by using SUMO®, a rapid aircraft geometry modeler. SUMO® is provided by Larosterna Engineering Dynamics. It is being developed as part of the EU funded SimSAC project (Eller, 2009).

In SUMO®, individual sections of aircraft can be designed on a modular basis, where the fuselage can be defined from its top and side view cross-sections and the wing can be modeled by defining airfoil sections at different spanwise locations. This rapid modeling capability of the software helped a lot during the current study. Several airfoil and wing incidence changes were implemented quickly and effectively. SUMO® also generates automatically an unstructured triangular surface mesh of the defined model. The surface mesh generated automatically follows the contour of the model and has variable mesh density depending on the bending of the surface (curvature). The surface mesh can be automatically generated but if needed it can also be refined manually.

A volume mesh around the surface mesh can also be created using the TetGen, developed by the Numerical Mathematics and Scientific Computing research group at Weierstrass Institute for Applied Analysis and Stochastics, Berlin. TetGen is a program to generate tetrahedral meshes of any 3D polyhedral domains (Si, 2009). By defining appropriate 3D volume mesh parameters a volume mesh can be created based on the surface mesh in SUMO®.

5.2.1 Modeling and Meshing in SUMO®

Using the rapid modeling techniques in SUMO®, a reference Airbus A320 wing and a box-wing were created. Only wing sections were modeled as modeling a complete aircraft was not considered suitable at this primary analysis phase.

Airfoil selection was an important task during the modeling procedure. For transonic wings the airfoil selection is dependent on cruise speed, wing sweep and design lift coefficient. All these parameters are known from reference aircraft data. Furthermore, selecting a particular

supercritical airfoil thickness to chord ratio is important. This thickness to chord ratio for this analysis was calculated using cruise Mach number and wing quarter chord sweep. First the cruise Mach number was selected equal to the drag divergence Mach number. This assumption is followed by both Airbus and Boeing (Scholz, 2007), where drag divergence Mach number is defined as: the Mach number where the coefficient of wave drag (that is additional drag due to Mach effects) amounts to 0.002.

Afterwards an effective drag divergence Mach number was calculated taking into account the wing quarter chord sweep by the following equation 5.4:

$$M_{DD_{eff}} = M_{DD}\sqrt{cos(\emptyset_{25})}$$

(5.4)

Thickness to chord ratio was computed using the equation (5.5) below (Scholz, 2007):

$$(t/c) = 0.3cos(\emptyset_{25})\left[\left\{1 - \left(\frac{5 + M_{DD_{eff}}^2}{5 + (k_m - 0.25C_L)^2}\right)^{3.5}\right\}\frac{\sqrt{1 - M_{DD_{eff}}^2}}{M_{DD_{eff}}}\right]^{2/3}$$

(5.5)

Where; t/c=thickness to chord ratio, $\emptyset_{25}$= Wing quarter chord sweep angle, $M_{DD_{eff}}$=effective drag divergence Mach number, k_m= 1.125 (for supercritical airfoils) and C_L=design lift coefficient

Thickness to chord ratio obtained from above equation amounts 0.11. Using this thickness to chord ratio and the design lift coefficient, NASA SC(2)-0710 or NASA SC(2)-0612 airfoils were selected as possible airfoils for both designs. Here it is important to choose a suitable airfoil for transonic analysis, as the compressibility drag due to high Mach numbers on the upper surface of the wing can affect the complete analysis.

Modeling the reference wing was a straight forward procedure. The twist values were taken from LAMDES results for both reference wing and box-wing. Choosing appropriate chord stations along span, the LAMDES calculated twist was implemented, although between each chord stations the variation of twist was linear. Final geometrical models of both types of wings having a surface mesh are shown in figure 5.1. The surface mesh created for this study had a mesh density of around 0.2 million triangles. Whereas the final volume mesh had a density of 1.7 million quadrilaterals. Considering the primary nature of the analysis, a 1.7 million mesh density was found suitable in comparison with other studies of similar nature using inviscid solvers (Andy, 2002).

38
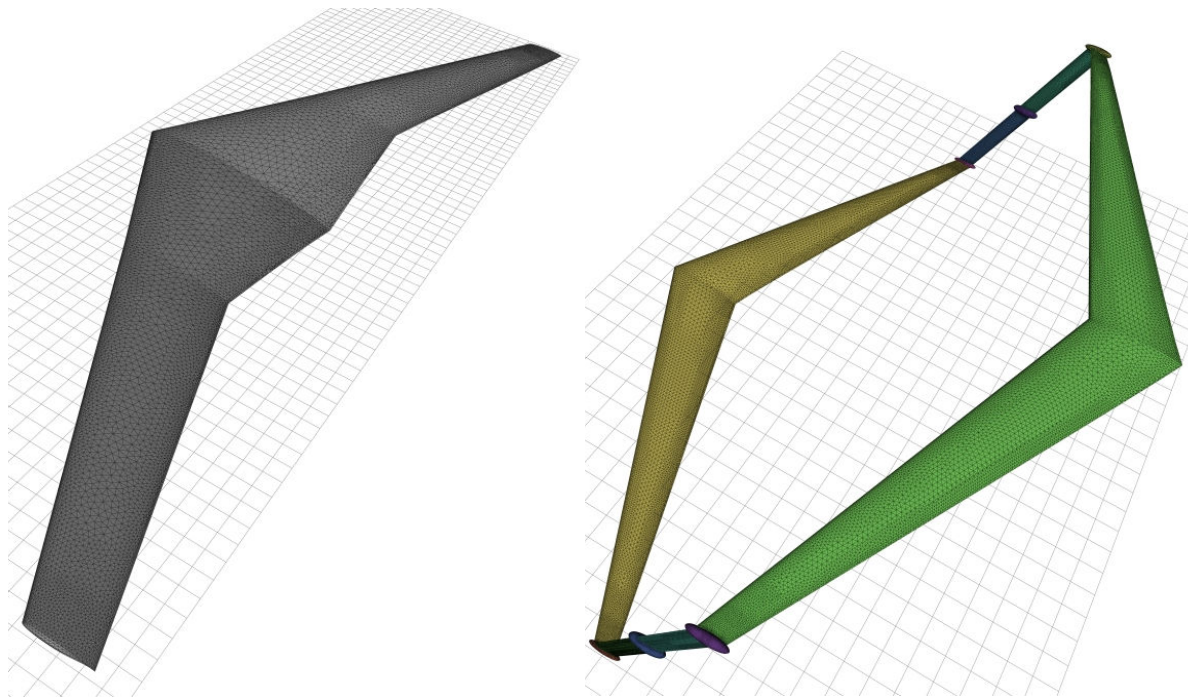
Figure 5.1 - Surface mesh created in SUMO for reference A320 wing (Right) selected box-wing configuration (Left)

5.3 EDGE® (Euler Solver)

Edge is a CFD flow solver for unstructured grids. It is developed by the Swedish Defense Research Agency (FOI) since 1997. It is very versatile code with the capability to solve compressible Reynolds-Averaged Navier-Stokes (RANS) equations with various state of the art turbulence models. It can also run compressible Euler and laminar solutions on hybrid grids.

The Edge flow solver is based on a node-centered finite volume scheme. For steady flows, the equations are integrated towards steady state with an explicit multi-stage Runge-Kutta scheme. To accelerate convergence, residual smoothing and a multi-grid technique can be employed. Low Mach-number preconditioning is also available. Time-accurate computations are implemented using dual time-stepping: implicit time marching with explicit sub-iterations (FOI, 2009).

5.3.1 Analysis with Edge Solver

Due to sensitive nature of the code, it is not completely available publicly. For current analysis only the Euler part of the code was utilized which is available as part of CEASIOM® software package (CFS, 2010). Euler capabilities of the EDGE® code are available via CEASIOM® but only initialization parameters can be adjusted along with reference values.

This limits the in depth execution of the Edge Code. The results obtained via EDGE® are written in Tecplot® format for visualization.

For inviscid drag comparison normally the design lift coefficient is equalized between different geometries. Using the LAMDES twist it was found the design lift coefficient of 0.67 was being achieved around 0° angle of attack. Thus, twist estimations were correct to some extent. For low subsonic (Mach number: 0.3) the reduction of induced drag was captured. While the drag obtained from different CFD runs at higher Mach numbers turned out to be higher than initially predicted as shown in table 5.1. The rise in coefficient of drag at transonic Mach number of 0.78 is due to the presence of strong shock waves over the wing surfaces thus causing an additional compressibility drag along with induced drag. These shocks can be seen in figures 5.2 and 5.3, which are displaying the Mach contours of the analyzed geometries.

Table 5.1 - Comparison of VLM and Euler method results

	C_{Di} from VLM	Difference	C_D from Euler Method (M=0.3)	Difference	C_D from Euler Method (M=0.78)	Difference
Reference A320 Wing	0.01467	-18.8%	0.01980	-12%	0.019857	+29%
Box-Wing	0.01191		0.017494		0.028002	

It is important to note here that the potential increase in compressibility drag is higher in the case of box-wing design. This result goes against the conclusions from (Miranda, 1972) which cited the decrease in compressibility drag applying box-wing configuration in her Patent on box-wing design in 1972. But here it should be mentioned that this study was conducted to see the potential aerodynamic advantage of the box-wing over conventional wing designs only in terms of induced drag reduction. Thus it doesn't cover any other form of drag reduction credibly.

The Mach contours for box-wing are shown in figure 5.3. According to the optimum span distribution required for maximum induced drag reduction, wing tips are heavily loaded. It can also be seen in the analysis below that the Mach number is considerably higher in tip regions due to the excessive incidence implemented in these regions.

Mach: 0.2 0.3 0.4 0.5 0.6 0.7 0.8 0.9 1 1.1 1.2 1.3 1.4 1.5
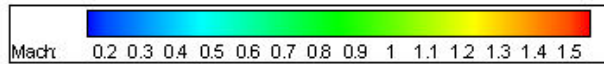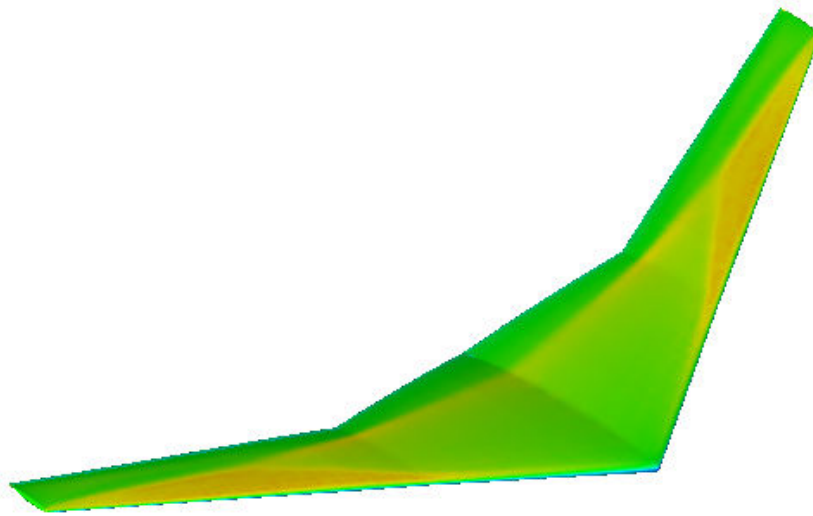
Figure 5.2 - Mach contours for reference A320 wing at cruise conditions

Mach: 0.1 0.2 0.3 0.4 0.5 0.6 0.7 0.8 0.9 1 1.1 1.2 1.3 1.4 1.5 1.6 1.7 1.8 1.9
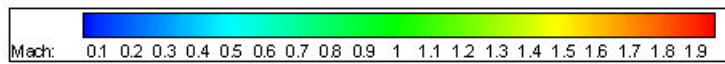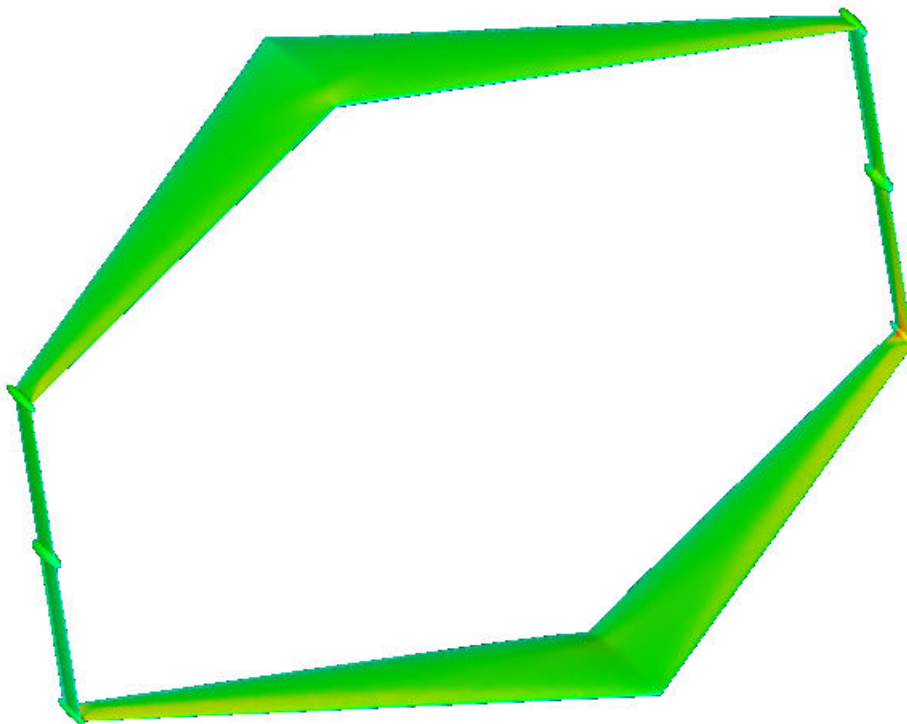
Figure 5.3 - Mach contours for selected box-wing configuration wing at cruise conditions

5.4 Conclusion

Results obtained from the Euler method were not completely accurate but the basic purpose of the analysis was accomplished. That is, the induced drag reduction for box-wing is shown compared to conventional designs.

Secondly, suitable airfoil selection came out to be an important issue in successful box-wing design. The supersonic flow over the box-wing configurations is not satisfactory and thus in future, airfoil selection can be added as major design issue for box-wing configuration.

6 Box-Wing Configuration and Aircraft Operations

This chapter outlines briefly the study done for the conclusion of this thesis work. Seeing prospects of drag reduction by utilizing a box-wing configuration, a possible operations and performance study was carried out.

Effects of choosing a box-wing commercial aircraft are studied for both, on and off ground scenarios for different categories of aircraft. It summarizes this in three separate sections. Possible advantages are highlighted. The study is completed with a short conclusion.

6.1 Aims of Study

Nowadays aircraft performance is not restricted to just improvement in cruise performance or short take-off and landing capabilities. With a growing number of air traffic, space congestion both on and off ground is becoming more vital than ever before. The success of a novel concept in future truly lies in all aspects of civil aircraft operations. At the current stage it would be almost economically impossible for aviation industry or the airport operators to adopt a completely new design having all-together different operational requirements. Similarly being a part of the *Airport 2030* project, it is important in this study to cover the aspects of box-wing design in the light of common airport issues.

Secondly, from the work done in previous chapters it can be concluded easily that there exists a credible potential decrease of induced drag for box-wing configuration. If for example, the selected box-wing configuration is chosen, it offers a minimum of total 10% reduction in complete drag as compared to existing conventional designs. Thus it can be easily proved by simple performance and mathematical equations that with a drag reduction of 10%, the cruise range would increase. Or maximum take-off weight can be increased. Similarly, aircraft emissions can be reduced too.

With all these positive factors, it was decided to outline all the aspects of box-wing aircraft operations and not just the in-flight performance improvements for different categories of civil transport aircraft. Thus in the following sections, instead of finding typical performance improvement values, a more general approach is followed, which covers the potential of box-wing design both in air and on ground as a potential regional airliner or a long endurance aircraft or as a very large aircraft concept.

6.2 Box-Wing Potential as a Regional Airliner

Regional airliners are certified under the design group III of Federal Aviation Administration (FAA) classification. Similarly, for International Civil Aviation Organization (ICAO) these

aircrafts are classified in design group C having a span limitation from 24m to 36m. This market is rapidly growing with the introduction of low-fare regional airlines. The two main aircrafts in this category are the Boeing 737 and the Airbus A320 (shown in figure 6.1 below along with an A320 box-wing concept).

The box-wing as a regional aircraft, it can surely perform better during cruise because of its higher lift to drag ratio. For the regional airliners, the aircraft perform several landings and take-offs during a single day and normally flight times are not very long. For such flight conditions, a box-wing aircraft can be a very appropriate solution, as induced drag gets higher at lower speeds in flight segments such as take-off, climb and landing, thus a box-wing aircraft which has the potential to reduce the induced drag can provide a more economical solution to this category of civil aviation aircraft.

Similarly, on the ground the biggest advantage someone gets out of a regional box-wing aircraft would be its commonality with existing aircrafts. As for these airlines long turns around periods are least desired so in the case of a box-wing aircraft, its fuselage has the same shape as conventional aircrafts. Thus it possesses no big risk in adapting to such missions. Similarly, as it has been shown earlier in this thesis, the considerable induced drag reduction can be achieved even if the aircraft total span is less than current conventional designs. So a box-wing regional aircraft can ease the parking space problem at airports as regional flights are increasing at a rapid rate. Seeing the different issues involving regional aircraft, a box-wing variant can be designed accordingly which favors operations of such airlines.

Figure 6.1 - Box-Wing variant of A320 (Left) and Airbus A320 (Courtesy Airbus) (Right)

Another aspect which is being looked into for a future regional aircraft, are aircrafts having high aspect ratios wings with less sweep than current designs. This helps to incorporate a natural laminar flow for drag reduction. Although these aircrafts are considered to be more economical then current aircrafts, the long slender wings will be a challenge when parking

space at terminals gets limited. In this category, a box-wing concept can also be studied as it might serve the same purpose and while the overall span can be much smaller.

6.3 Box-Wing Potential as a Long Endurance Aircraft

Recently long endurance aircrafts have got a lot attention. The two upcoming aircrafts the Boeing 787 and Airbus the A350 would lie in this category. According to ICAO this class falls into the design group E with span limitations from 52m to 65m.

To achieve high endurance for such aircraft extra long span is required. High aspect ratio wings are serving best for this purpose. As noted earlier in the literature review section, high aspect ratio wings have two main problems. First, with increase in span the wing weight increases. Secondly, practical problems occur during ground operations for aircraft with very high span. A box-wing long endurance aircraft can possibly eliminate both of the problems. According to recent research the box-wing aircraft might even prove to be structurally stiffer than conventional designs thus allowing higher aspect ratios for individual wings of the box-wing design (Cranfield, 2010).

6.4 Box-Wing Potential as a Very Large Aircraft

As the volume of air passengers grow rapidly the aviation industry has keen interest in this category of civil aircrafts. Very Large Aircraft (VLA) have been under investigation for several years now. The Airbus A380 already belongs to this category of aircraft which is classified by ICAO as design group F having span limitations equal to or greater than 65m. The only aircraft which goes currently beyond the 80x80m box limit is the Antonov An225.

For upcoming VLA designs, airport operations and compatibility plays an important role. According to Airbus, the Airbus A380 was designed to minimize the changes required to operate it from existing airports (Rosenkrans, 2007). As the A380 span is just short of 80m limit, thus in future if a similar but bigger aircraft than A380 is going to be manufactured than the airport terminals around the world would have to be modified heavily to accommodate such an aircraft. The answer for this problem can lie in the box-wing design. The box-wing can accommodate higher passenger capacity than an A380 but still have similar or even smaller overall span.

Also as the passenger number grows, double deck aircraft are more favored because of their potential advantage in having less drag. As for double deck aircraft, the increase in fuselage wetted area is considerably less as compared to a single deck aircraft having same increase in passenger capacity. In a box-wing design, a double deck fuselage is favored as it can provide

more strength to the two main wings while maintaining a good height to span ratio for the complete design.

When it comes to airport compatibility and operations the VLA concepts can face major hurdles. Another aspect in which a box-wing VLA can beneficial is the maneuver envelope available at current airport. Similarly, the extensions of taxiways and runways can be avoided by choosing a much smaller span box-wing VLA. As mentioned earlier, a box-wing configuration can take advantage of its conventional fuselage design to ease up the passenger loading and offloading procedures. Similarly, ground handling and emergency requirements would be much easier to fulfill by selecting a box-wing VLA. As compared to other VLA concepts, like blended wing body design, a box-wing offers much more ease and simplicity in ground operations.

Another important factor that originates more profoundly with the VLA class is wake vortex limitations. As these heavy aircrafts require immense amount of lift to take-off thus if conventional designs are followed than it will pose higher restrictions for time intervals between consecutive take-offs. In box-wing design one of the important features is the reduction of vortex drag. Thus, for a box-wing VLA the wake vortex limitations can be eased up considerably. There are similar other restrictions for example engine span to wing span limitations and engine ground clearance limitations. These can be also eased up with proper installation of engines in a box-wing VLA as it offers various locations for effective engine installation.

6.5 Noise and Emissions

The reduction in noise and emissions are major goals for future air travel. By choosing the novel concepts like box-wing having improved power plant design can provide a way to reduce both emissions and noise. Lesser drag means lesser power requirements, thus lesser impact on the environment through emissions. Similarly, noise can be reduced by shielding the engines in the aft fuselage section between the twin vertical fins. Several other engine installation options are available in a box-wing if further explored.

6.6 Conclusion

During this brief study it was concluded that several benefits exist in opting for a box-wing aircraft. These benefits are not limited to only in-flight performance improvements. Several ground based operational aspects of the box-wing aircraft are present which can be made into an advantage.

Also if a complete design study of this type of aircraft is made, it will be useful not in terms of a single type of civil aircraft. Several successful versions can be made starting from regional size and going up to very large scale.

It can be concluded here too, that the designing of such an aircraft should include both on and off design requirements as only in this way a real benefit can be obtained.

7 Conclusion and Summary

Nonplanar systems do posses the capabilities to reduce the induced drag significantly. It can be concluded that this reduction is mainly due to overall reduction in the downwash of the complete system. The increase in aspect ratio by dividing a surface into two or more similar span surfaces having same total wing area can considerably reduce the induced drag. In addition to this it is seen that by adding a winglet or an endplate to a lifting system further reduces the downwash and increases the overall span efficiency of the system.

For the analysis of nonplanar systems, vortex lattice codes can be utilized. Here two important conclusions can be drawn from this work. First, appropriate span loading should be established and maintained throughout the analysis of a nonplanar system. The span loading can be of any shape depending upon the system under consideration. Secondly, during this analysis care must be taken while defining span efficiency and aspect ratio of the individual lifting surfaces and as a whole for the complete lifting system. If not defined properly, it may result in wrong values and lead to incorrect conclusions afterwards.

As far as the box-wing design variables are concerned, the stagger, sweep and taper ratio has no effect on the complete induced drag of the system if adequate span loading is maintained. While, induced drag increases with an introduction of a dihedral upon the system. Furthermore, height to span ratio is the most important variable which directly influences the overall efficiency. Further improvement can be made by adjusting the cant angles for winglets.

Although the twist calculations carried in LAMDES were not corresponding to supercritical airfoils and the analysis carried out by Euler code was of preliminary nature it still provided a good insight into the box-wing design. Transonic airfoil selection is identified as one of the important design variables. Further work should still be done in this domain to remove any ambiguities and to further identify any remaining aerodynamic challenges.

During operation, a box-wing as a very large aircraft seems to be the most appropriate application, as it can prove to be a good solution for the ground operational problems and at the same time minimizing low Reynolds number effects in the box-wing VLA case.

Furthermore, viscous effects were neglected in this analysis. These effects should however be investigated and taken into consideration for a more detailed analysis. As early stated, a box-wing concept can be truly analyzed by performing a coupled analysis of aerodynamic, structure and stability calculations. After such an analysis the true potential of the box-wing design can be evaluated more accurately.

List of References

A. Frediani, e. a. (2005). A 250 Passenger Prandtl Plane Transport Aircraft. *XVIII CONGRESSO NAZIONALE AIDAA.*

Anderson, J. D. (1999). *Aircraft Performance and Design.*

Anderson, J. D. (1995). *Computational fluid dynamics.*

Anderson, J. D. (2001). *Fundamentals of Aerodynamic (3rd Edition).* New York: McGraw-Hill.

Andy, K. e. (2002). *A-7 strut braced wing concept transonic wing design.* Department of Aerospace and Ocean Engineering, Virginia Polytechnic Institute and State University.

Blackwell, J. A. (1976). *Numerical Method to Calculate the Induced Drag or Optimum Loading for Arbitrary Non-Planer Aircraft.* NASA Langley Research Center.

CFS, E. (2010). *CFS Engineering.* Retrieved March 2010, from CEASIOM: Computerised Environment for Aircraft Synthesis and Integrated Optimisation Methods: http://www.ceasiom.com/

Collins, T. D. (2001). *Analysis of A380 Transport.* Retrieved 2010, from http://www.aoe.vt.edu/~mason/Mason_f/A380Collins.pdf

Cranfield, U. (2010). *The Design of a Novel Box-Wing Medium Range Airliner: The A-9 Dragonfly.* Retrieved March 2010, from Cranfield University: http://www.cranfield.ac.uk/soe/departments/aerospaceengineering/page47131.html

DeYoung, J. (1976). *Historical Evolution of Vortex-Lattice Methods.*

Eller, D. (2009). *Aircraft modeling and mesh generation.* Retrieved March 2010, from Larosterna Engineering Dynamics: http://www.larosterna.com/sumo.html

Ferziger, J. P. (2002). *Computational methods for fluid dynamics.*

FOI. (2009). *Edge.* Retrieved March 2010, from Swedish Defence Research Agency: http://www.foi.se/FOI/Templates/ProjectPage_____4690.aspx

Frediani A, e. a. (2005). *A 250 passenger prandtlplane transport aircraft preliminary design.* AIDAA.

Frediani A, e. a. (2003). *Development of an innovative configuration for transport aircraft; a project of five Italian universities.*

Frediani A., M. G. (1999). *Best Wing System: An Exact Solution of the Prandtl's Problem.* Variational Analysis and Aerospace Engineering - Springer Optimization and Its Applications 33.

Frediani, A. e. (2006). *The Prandtl Plane Aircraft Configuration.*

Gall, P. D. (1984). *An Experimental and Theoratical Analysis of the Aerodynamic Characteristics of a Biplane-Winglet Configuration.* NACA TM 85815.

Grasmeyer, J. (1997). *A Discrete Vortex Method for Calculating the Minimum Induced Drag and Optimum Load Distribution for Aircraft Configurations with Noncoplanar Surfaces.* Department of Aerospace and Ocean Engineering, Virginia Polytechnic Institute and State University.

Holland, J. (1975). *Adaption in natural and artificial systems.* University of Michigan Press, Ann Arbor.

Jackson, P. (2009). *Jane's all the world aircraft.* Janes.

Jones, R. T. (1950). *The Spanwise Distribution of Lift for Minimum Induced Drag of Wings having a Given Lift and a Given Bending Moment .* NACA TN 2249.

Kroo, I. (2006). *Aircraft Design: Synthesis and Analysis.* Desktop Aeronautics, Inc (http://adg.stanford.edu/aa241/welcome.html).

Kroo, I. (2000). *Design and development of the SWIFT: a foot-launched sailplane.* AIAA-00-4336.

Kroo, I. (2001). Drag Due to Lift: Concepts for Prediction and Reduction. *Annual Review Fluid Mechanics* , 587-617.

Kroo, I. (2005). Nonplanar Wing Concepts For Increased Aircraft Efficiency. *VKI lecture series on Innovative Configurations and Advanced Concepts for Future Civil Aircraft .*

Mason, W. H. (1995). *Applied computational aerodynamics text/notes.* Retrieved April 2010, from http://www.aoe.vt.edu/~mason/Mason_f/CAtxtTop.html

McMasters J, K. I. (1998). *Advanced configuration for very large transport airplanes.* Aircr.Des. 1:217–42.

Miranda, L. (1972). *Boxplane configuration, conceptual analysis and initial experimentation.* LR 25180, Lockheed California.

Munk, M. (1921). *The Minimum Induced Drag of Aerofoils.* NACA Rep.121.

Obert, E. (2009). *Aerodynamic design of transport aircraft.*

P. Busquin, P. A.-L. (January 2001). *European Aeronatics: A Vision For 2020.*

Prandtl, L. (1924). *Induced Drag of Multiplanes.* NACA TN 182.

Raymer, D. P. (1992). *Aircraft design: A conceptual approach.* American Institute of Aeronautics and Astronautics, Inc., Washington, DC.

Rosenkrans, W. (2007, July). Airport Ops. *Aero Safety World, Flight Safetly Foundation* .

Scholz, D. (2007). *Short Course: Aircraft Design.* Berlin: DGLR.

Si, H. (2009). *TetGen - A Quality Tetrahedral Mesh Generator and a 3D Delaunay Triangulator.* Retrieved March 2010, from http://tetgen.berlios.de/

Smith, H. (2008). Novel Aircraft Concepts to Reduce Noise and Global Warming Effects. *ICAS-26TH International Congress of the Aeronautical Sciences.*

Strang, W. a. (1979). Concorde in Service. *Aeronautical Journal* .

Stuart, R., & Peter, N. (2003). *Artificial Intelligence: A Modern Approach (2nd Edition).* Prentice Hall Series.

Terry, J. (1964). *Aerodynamic characteristics of ring wings: a bibliography.* RSIC-285.

Tomas, M. (2000). *A vortex lattice MATLAB implementation for linear aerodynamic wing applications.* Royal Institute of Technology (KTH).

Torenbeeck, E. (2005). Introduction to overview of innovatice civil trasnport configurations. *Lecture Series: Innovative configurations and advanced concept for future civil aircraft.* Von Karman Institute .

Whitcomb, R. (1976). *A design approach and selected wind tunnel rsults at high subsonic speeds for wing-tip mounted winglets.* NASA TN D-8260.

Wolkovitch, J. (1986). *The joined wing: an overview.* AIAA J.Aircr. 23:161–78.

Appendix A – Tornado Results
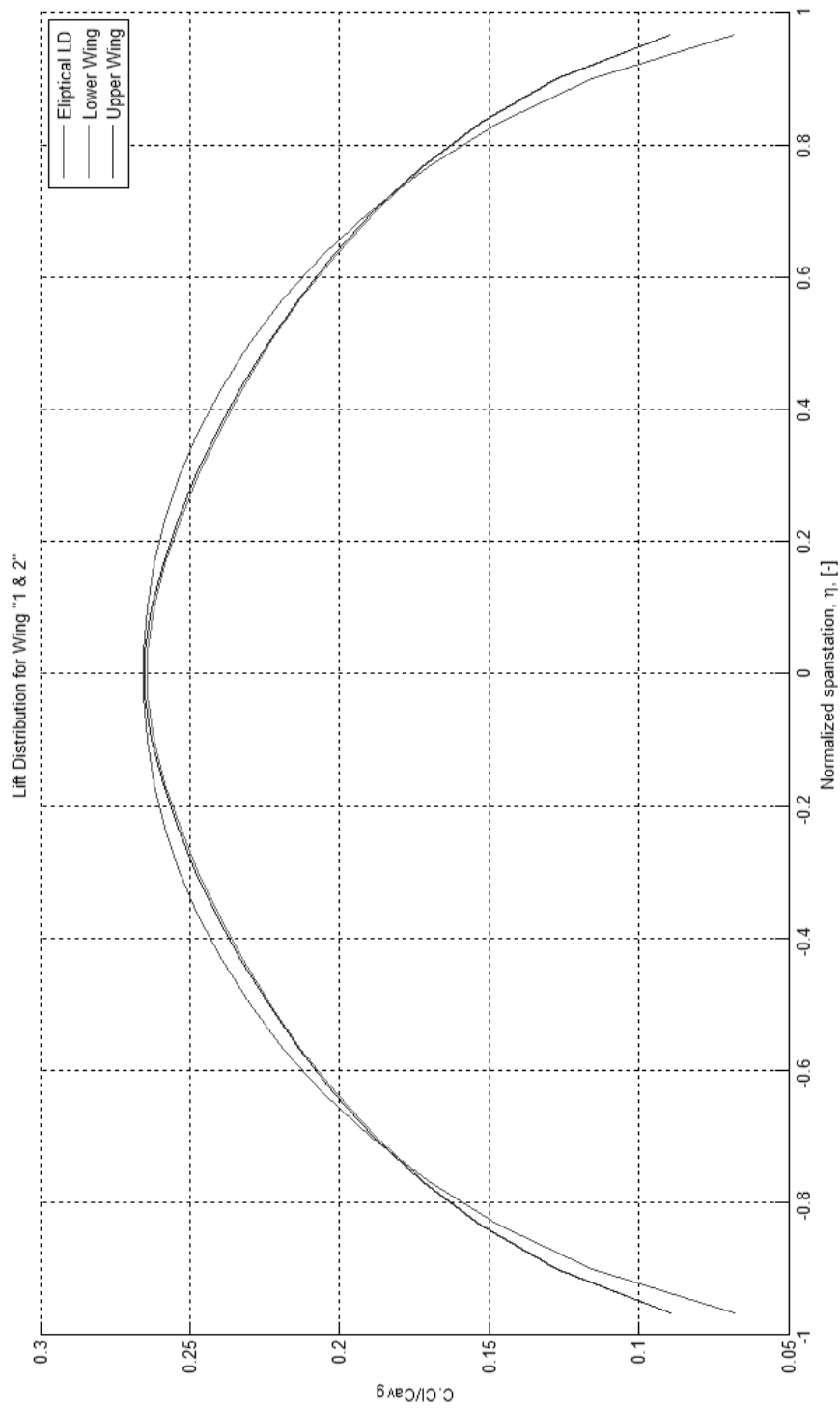
Figure A.1 - Spanwise load distribution for unstaggered wings obtained from Tornado VLM
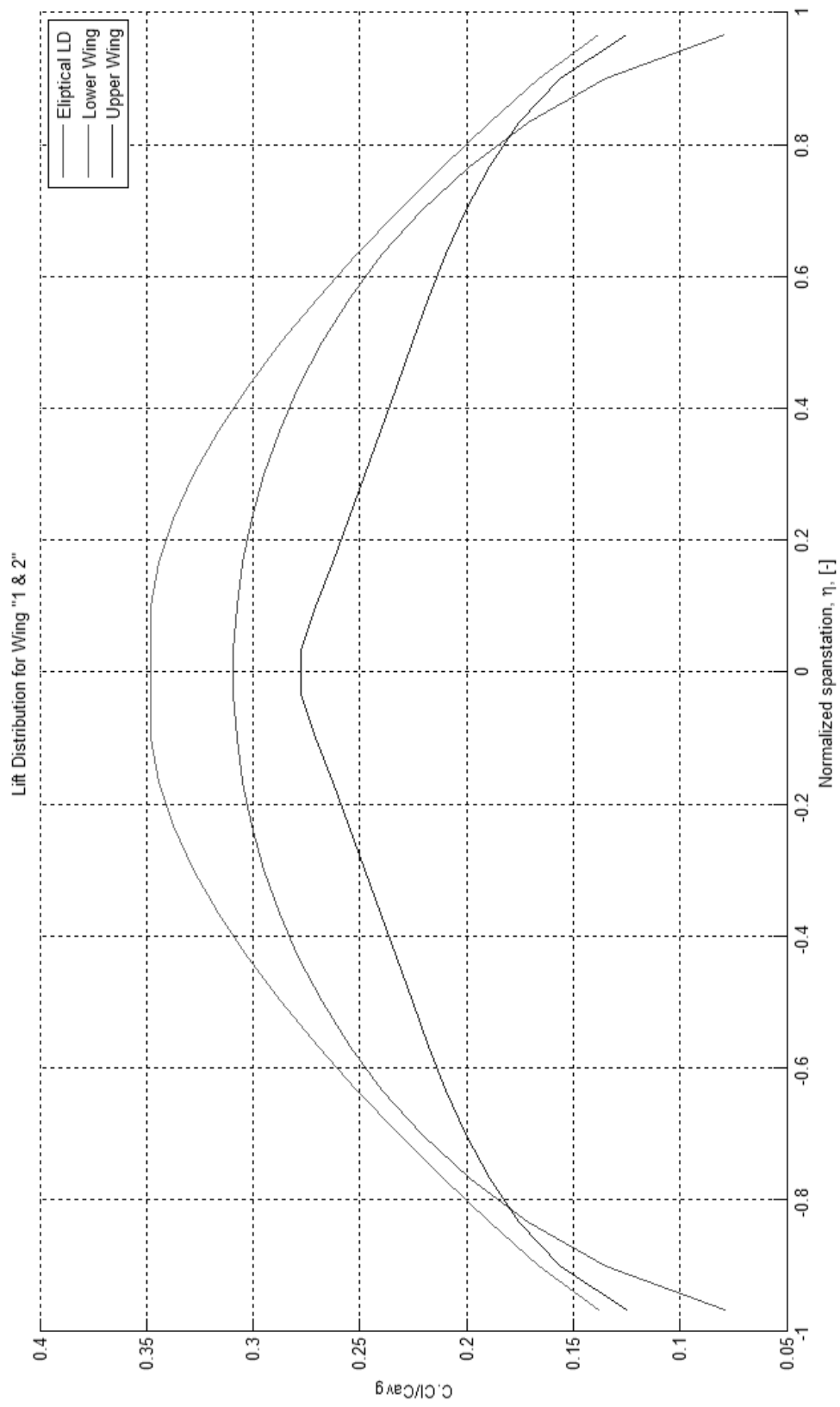
**Figure A.2 - Spanwise load distribution for staggered wings obtained from Tornado VLM**

Appendix B – CFD Plots
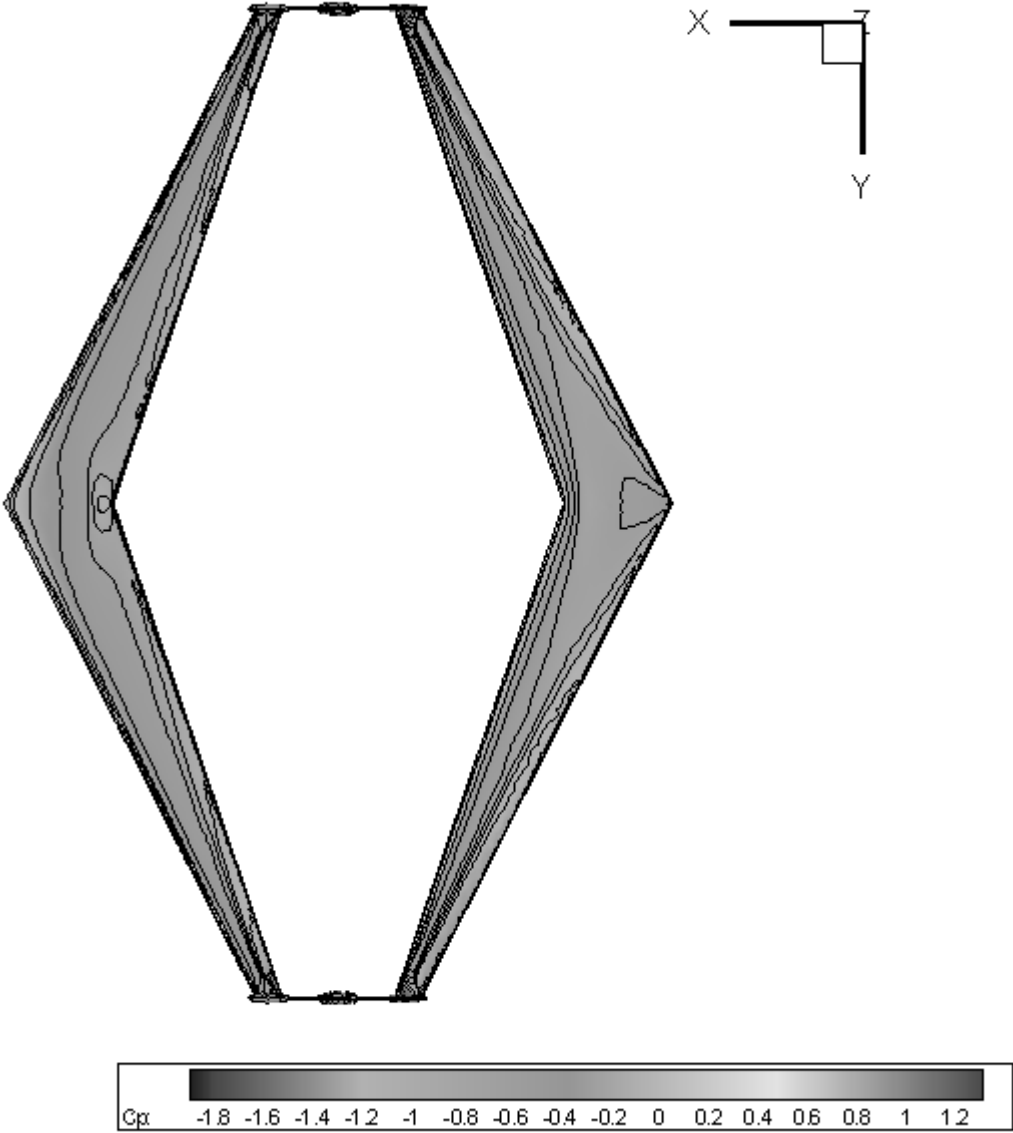
Figure B.3 - Cp distribution of box-wing configuration (Top View)
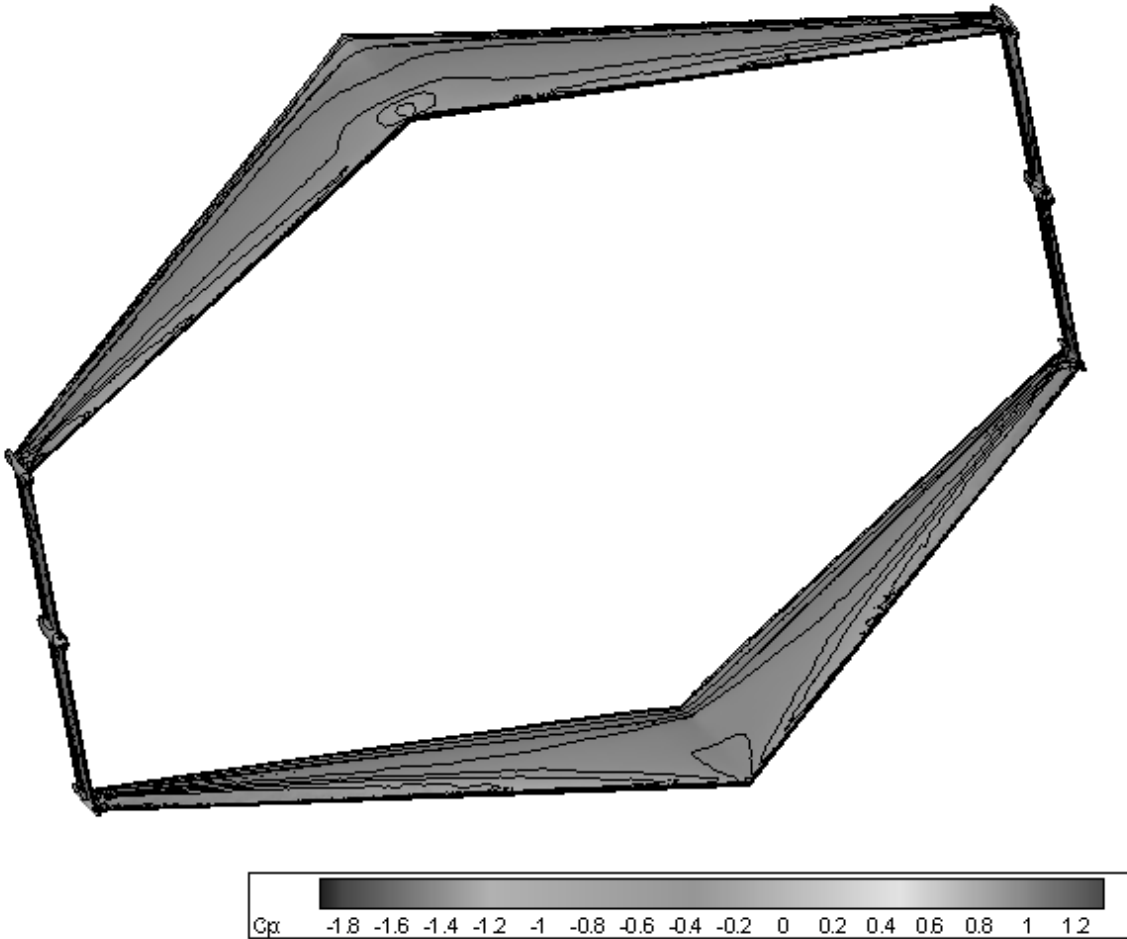
**Figure B.4 - Cp distribution of box-wing configuration (Asymmetric View)**
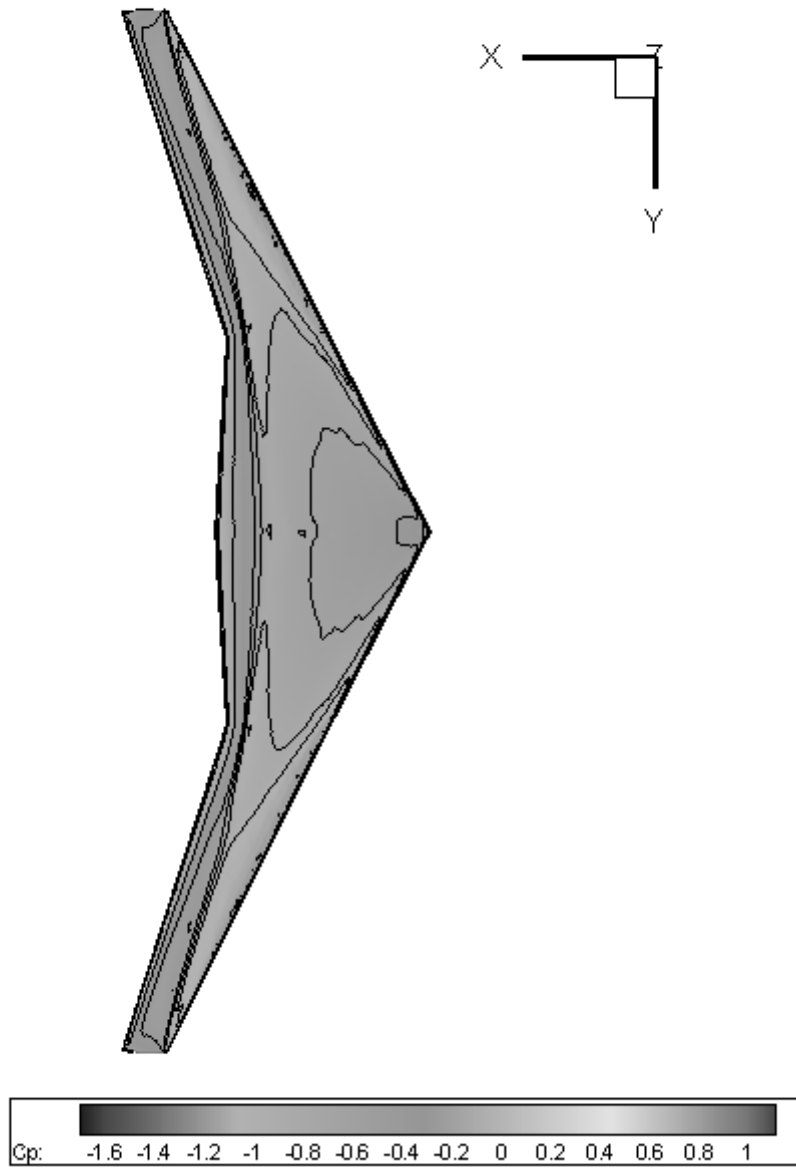
**Figure B.5 - Cp distribution for reference A320 wing (Top View)**
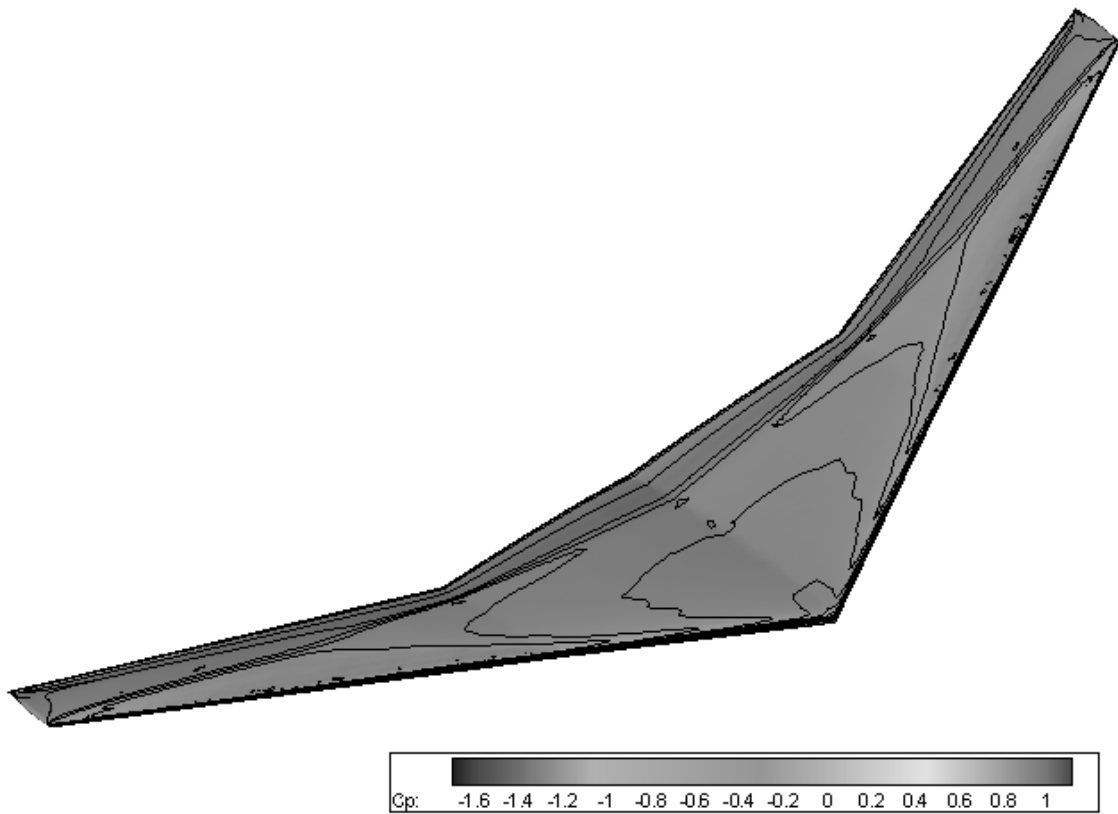
Figure B.6 - Cp distribution for reference A320 wing (Asymmetric View)

Appendix C – IDRAG_in.m Script

```
function
[e]=IDRAG_in(AR,lamda1,lamda2,dih1,dih2,sw1,sw2,hb,stg,ref_S,ref_CL,cant)
%IDRAG_in Creates input file for idrag on given configuration geometry.
%
%     IDRAG_in(INPUT PARAMETERS)
%       Parameter Details:
%           ref_S   = Combined reference area of both wings (m^2)
%           ref_CL  = Design lift coefficient
%           lamda1  = Taper Ratio of Wing 1
%           lamda2  = Taper Ratio of Wing 2
%           dih1    = Dihedral (+/-) Wing 1 (Degrees)
%           dih2    = Dihedral (+/-) Wing 2 (Degrees)
%           sw1     = Quarter Chord Sweep Wing 1 (Degrees)
%           sw2     = Quarter Chord Sweep Wing 2 (Degrees)
%           hb      = height/span ratio
%           AR      = Single Value taken for both wings
%           stag    = Stagger, used in multiple of Wing1 MAC
%           cant    = Cant angle for winglets (+ve outward)
%     If idrag is called with just XXX argument, ref_S and ref_cl
%     are set to their default values of 122.2 and 0.67 respectively.
%        Wing 1 is always "Bottom Wing"
%        Wing 2 is always "Top Wing"
%
% Written by F A Khan on 12/03/10 @ HAW-Hamburg

% Calculating Span for both individual wings
b=sqrt(AR*(ref_S/2));

% Calculating Root, Tip & MAC Chords for Wing 1
Cr1=(ref_S/2)/(b*(lamda1));
Ct1=lamda1*Cr1;

MAC=(ref_S)/b;

% Calculating Root, Tip & MAC Chords for Wing 2
Cr2=(ref_S/2)/(b*(lamda2));
Ct2=lamda2*Cr2;

% Calculating Box Height
bh=hb*b;

% Stagger
stag=stg*(MAC)/2;

% Dihedral for Wing 1 & 2
di_1=sin(dih1*0.017453293)*b/2;
di_2=sin(dih2*0.017453293)*b/2;

% Sweep (LE) for Wing 1 & 2
sw1_LE=atan(tan(sw1*0.017453293)+((1-lamda1)/(AR*(1+lamda1))));
x_sw_1=tan(sw1_LE)*b/2;
```

```matlab
sw2_LE=atan(tan(sw2*0.017453293)+((1-lamda2)/(AR*(1+lamda2))));
x_sw_2=tan(sw2_LE)*b/2;

% Adjusting Cant Angle for Winglet tips
cant_1=tan(cant*0.017453293)*((bh-di_2-di_1)/2);


fid=fopen('D:\BW\Work\Softwares\idrag\My work\Matlab\cas.in','w');
fprintf(fid,'%s\n','idrag input file');
fprintf(fid,'BW_Optimizer\n');
fprintf(fid,'%g                 %s\n',0,'input mode');
fprintf(fid,'%g                 %s\n',1,'write flag');
fprintf(fid,'%g                 %s\n',1,'symmetry flag');
fprintf(fid,'%g                 %s\n',ref_CL,'cl_design');
fprintf(fid,'%g                 %s\n',0,'cm_flag');
fprintf(fid,'%g                 %s\n',0,'cm_design');
fprintf(fid,'%g                 %s\n',6.71,'x cg position');
fprintf(fid,'%g                 %s\n',0.25,'center of pressure for airfoil
sections');
fprintf(fid,'%g                 %s\n',ref_S,'reference area');
fprintf(fid,'%g                 %s\n',MAC,'reference chord');
fprintf(fid,'%g                 %s\n',4.0,'number of panels');


%panel 1 - Lower Main Wing
fprintf(fid,'%g   %g   %g       %s\n',0,0,0,'x,y,z for 4 corners of panel
1'); % Origin as Wing 1 Root tip point
    % Wing 1 Point 2
    W1_Pt2_x=x_sw_1;
    W1_Pt2_y=b/2;
    W1_Pt2_z=di_1;
fprintf(fid,'%g   %g   %g       \n',W1_Pt2_x,W1_Pt2_y,W1_Pt2_z);
    % Wing 1 Point 3
    W1_Pt3_x=x_sw_1+Ct1;
    W1_Pt3_y=b/2;
    W1_Pt3_z=di_1;
fprintf(fid,'%g   %g   %g       \n',W1_Pt3_x,W1_Pt3_y,W1_Pt3_z);
fprintf(fid,'%g   %g   %g       \n',Cr1,0,0);
fprintf(fid,'%g                 %s\n',30,'number of vortices for panel 1');
fprintf(fid,'%g                 %s\n',0,'vortex spacing for panel 1');


%panel 2 - Upper Main Wing
    % Wing 2 Point 1
    W2_Pt1_x=stag;
    W2_Pt1_y=0;
    W2_Pt1_z=bh;
fprintf(fid,'%g   %g   %g       %s\n',W2_Pt1_x,W2_Pt1_y,W2_Pt1_z,'x,y,z for 4
corners of panel 2');
    % Wing 2 Point 2
    W2_Pt2_x=stag+x_sw_2;
    W2_Pt2_y=b/2;
    W2_Pt2_z=bh+di_2;
fprintf(fid,'%g   %g   %g       \n',W2_Pt2_x,W2_Pt2_y,W2_Pt2_z);
    % Wing 2 Point 3
    W2_Pt3_x=stag+Ct2+x_sw_2;
    W2_Pt3_y=b/2;
```

```matlab
    W2_Pt3_z=bh+di_2;
fprintf(fid,'%g   %g   %g      \n',W2_Pt3_x,W2_Pt3_y,W2_Pt3_z);
    % Wing 2 Point 4
    W2_Pt4_x=stag+Cr2;
    W2_Pt4_y=0;
    W2_Pt4_z=bh;
fprintf(fid,'%g   %g   %g      \n',W2_Pt4_x,W2_Pt4_y,W2_Pt4_z);
fprintf(fid,'%g                %s\n',30,'number of vortices for panel 2');
fprintf(fid,'%g                %s\n',0,'vortex spacing for panel 2');


%panel 3 - Lower Winglet
fprintf(fid,'%g   %g   %g      %s\n',W1_Pt2_x,W1_Pt2_y,W1_Pt2_z,'x,y,z for 4
corners of panel 3'); % same as Wing 1 Pt 2
fprintf(fid,'%g   %g   %g      \n',(W1_Pt2_x+(W2_Pt2_x-
W1_Pt2_x)/2),(W2_Pt2_y+cant_1),(W2_Pt2_z-W1_Pt2_z)/2+W1_Pt2_z);
fprintf(fid,'%g   %g   %g      \n',(W1_Pt3_x+(W2_Pt3_x-
W1_Pt3_x)/2),(W2_Pt2_y+cant_1),(W2_Pt2_z-W1_Pt2_z)/2+W1_Pt2_z);
fprintf(fid,'%g   %g   %g      \n',W1_Pt3_x,W1_Pt3_y,W1_Pt3_z); % same as
Wing 1 Pt 3
fprintf(fid,'%g                %s\n',7,'number of vortices for panel 3');
fprintf(fid,'%g                %s\n',0,'vortex spacing for panel 3');


%panel 4 - Upper Winglet
fprintf(fid,'%g   %g   %g      \n',(W1_Pt2_x+(W2_Pt2_x-
W1_Pt2_x)/2),(W2_Pt2_y+cant_1),(W2_Pt2_z-W1_Pt2_z)/2+W1_Pt2_z); % same as
Winglet lower Pt 2
fprintf(fid,'%g   %g   %g      \n',W2_Pt2_x,W2_Pt2_y,W2_Pt2_z); % same as
Wing 2 Pt 2
fprintf(fid,'%g   %g   %g      \n',W2_Pt3_x,W2_Pt3_y,W2_Pt3_z); % same as
Wing 2 Pt 3
fprintf(fid,'%g   %g   %g      \n',(W1_Pt3_x+(W2_Pt3_x-
W1_Pt3_x)/2),(W2_Pt2_y+cant_1),di_1+(W2_Pt2_z-W1_Pt2_z)/2+W1_Pt2_z); % same
as Winglet lower Pt 3
fprintf(fid,'%g                %s\n',7,'number of vortices for panel 3');
fprintf(fid,'%g                %s\n',0,'vortex spacing for panel 3');
fclose(fid);

% Calling script for running Idrag
system('D:\BW\Work\Softwares\idrag\My work\Matlab\idrag_script.au3');
% Reading Idrag Output file for "e"
fid = fopen('casout2.rtf','r');
str = fscanf(fid,'%c');
ms = char(str);
k = strfind(ms, 'induced drag coefficient');
S = strtrim(ms(k(1)-10:k(1)-3));
CDi = str2double(S)
n = strfind(ms, 'span efficiency factor');
O = strtrim(ms(n(1)-10:n(1)-3));
e = str2double(O)
fclose(fid);

----------------------------------------------------------------
```

Appendix D – IDRAG GCA Script

```matlab
%****
%*********Optimizer Code for Box-Wing Aircraft based on Idrag Code*********
%****
%****
%     BW_OPT(INPUT PARAMETER=None)
% The code defines different box wing parameters and there variation
% limits. Forwards this information to IDRAG_in.m which computes "e".
% Optimization technique: CGA
%        Parameter Details:
%            ref_S   = Combined reference area of both wings (m^2)
%            ref_CL  = Design lift coefficient
%            lamda1  = Taper Ratio of Wing 1
%            lamda2  = Taper Ratio of Wing 2
%            dih1    = Dihedral (+/-) Wing 1 (Degrees)
%            dih2    = Dihedral (+/-) Wing 2 (Degrees)
%            sw1     = Quarter Chord Sweep Wing 1 (Degrees)
%            sw2     = Quarter Chord Sweep Wing 2 (Degrees)
%            hb      = height/span ratio
%            AR      = Single Value taken for both wings
%            stag    = Stagger, used in multiple of Wing1 MAC
%         Wing 1 is always "Bottom Wing"
%         Wing 2 is always "Top Wing"
%
% Written by F A Khan on 15/03/10 @ HAW-Hamburg


clc


% Defining the reference values
AR=9.5;          % Aspect Ratio of individual wing of box wing
ref_S=122.4;     % Reference area of combined wings
ref_CL=0.67;     % Design Lift Coefficient
stg=5;           % Negative stagger multiple of Mean MAC of both wings


var = 51;
% Initializing Taper Ratios
lamda1=0.1:0.018:1;
lamda2=0.1:0.018:1;

% Initializing Dihedrals
dih1=0:0.2:10;
dih2=-10:0.2:0;

% Initializing Sweep
sw1=0:0.7:35;
sw2=-35:0.7:0;

% Initializing Height to Span Ratio
hb=0.01:0.0078:0.4;

% Making 10 Random Parents
R=round(randperm(var));
```

```
for n=1:10
    Prt(n,1)=lamda1(R(n));
    Prt(n,2)=lamda2(R(n));
    Prt(n,3)=dih1(R(n));
    Prt(n,4)=dih2(R(n));
    Prt(n,5)=sw1(R(n));
    Prt(n,6)=sw2(R(n));
    Prt(n,7)=hb(R(n));
end

Max_Itre=100;
Iter=100;

for glob=1:Max_Itre

    % Passing above Parent to Idrag for efficiency computation
    for n=1:10

e(n)=IDRAG_in(AR,Prt(n,1),Prt(n,2),Prt(n,3),Prt(n,4),Prt(n,5),Prt(n,6),...
        Prt(n,7),stg,ref_S,ref_CL);
    end
    e
    % Sorting for best 5 Parents
    [B,IX]=sort(e,'descend');

    % Copying 5 best parents in first 5 Prt cells
    for n=1:5
        Prt(n,1)=Prt(IX(n),1);
        Prt(n,2)=Prt(IX(n),2);
        Prt(n,3)=Prt(IX(n),3);
        Prt(n,4)=Prt(IX(n),4);
        Prt(n,5)=Prt(IX(n),5);
        Prt(n,6)=Prt(IX(n),6);
        Prt(n,7)=Prt(IX(n),7);
    end

    % Crossover for bad 5 parents
    for n=1:5
        R=round(randperm(5));
        Prt(n+5,1)=Prt(R(1),1);
        Prt(n+5,2)=Prt(R(3),2);
        Prt(n+5,3)=Prt(R(4),3);
        Prt(n+5,4)=Prt(R(1),4);
        Prt(n+5,5)=Prt(R(2),5);
        Prt(n+5,6)=Prt(R(5),6);
        Prt(n+5,7)=Prt(R(3),7);
    end

    % Mutation in New Parents
    R_all=round(randperm(var));
    R_small=round(randperm(7)+3);

        Prt(R_small(1),1)=lamda1(R_all(30));
        Prt(R_small(4),2)=lamda2(R_all(12));
```

```
        Prt(R_small(7),3)=dih1(R_all(49));
        Prt(R_small(5),4)=dih2(R_all(43));
        Prt(R_small(6),5)=sw1(R_all(25));
        Prt(R_small(3),6)=sw2(R_all(4));
        Prt(R_small(2),7)=hb(R_all(8));

    e_tot(glob)=B(1);
    Iter(glob)=glob;

end

disp(['The value of Lamda 1    for Wing 1 is: ',num2str(Prt(1,1))]);
disp(['The value of Lamda 2    for Wing 2 is: ',num2str(Prt(1,2))]);
disp(['The value of Dihedral 1 for Wing 1 is: ',num2str(Prt(1,3))]);
disp(['The value of Dihedral 2 for Wing 2 is: ',num2str(Prt(1,4))]);
disp(['The value of Sweep 1    for Wing 1 is: ',num2str(Prt(1,5))]);
disp(['The value of Sweep 2    for Wing 2 is: ',num2str(Prt(1,6))]);
disp(['The value of Height to Span Ratio   for Box-Wing is:
',num2str(Prt(1,7))]);
disp(['The value of Span Efficiency Factor for Box-Wing is:
',num2str(e(1))]);

% Plotting Result
plot(Iter,e_tot);
title('Variation of Span Efficiency Factor for Box-Wing');
grid on;
ylabel('Span Efficiency Factor');
xlabel('Number of Iterations');


-------------------------------------------------------------------------
```